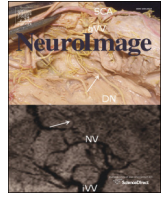




Contents lists available at SciVerse ScienceDirect

NeuroImage

journal homepage: www.elsevier.com/locate/ynimg

Review

Time domain functional NIRS imaging for human brain mapping[☆]Alessandro Torricelli^{a,*}, Davide Contini^a, Antonio Pifferi^a, Matteo Caffini^b, Rebecca Re^a, Lucia Zucchelli^a, Lorenzo Spinelli^c^a Politecnico di Milano, Dipartimento di Fisica, piazza Leonardo da Vinci 32, I-20133, Milan, Italy^b Politecnico di Milano, Dipartimento di Elettronica, Informazione e Bioingegneria, via Golgi 39, I-20133, Milan, Italy^c Istituto di Fotonica e Nanotecnologie, Consiglio Nazionale delle Ricerche, piazza Leonardo da Vinci 32, I-20133, Milan, Italy

ARTICLE INFO

Article history:

Accepted 21 May 2013

Available online xxxx

Keywords:

Functional near-infrared spectroscopy

Time domain

Continuous wave

Instrumentation

Penetration depth

Depth selectivity

ABSTRACT

This review is aimed at presenting the state-of-the-art of time domain (TD) functional near-infrared spectroscopy (fNIRS). We first introduce the physical principles, the basics of modeling and data analysis. Basic instrumentation components (light sources, detection techniques, and delivery and collection systems) of a TD fNIRS system are described. A survey of past, existing and next generation TD fNIRS systems used for research and clinical studies is presented. Performance assessment of TD fNIRS systems and standardization issues are also discussed. Main strengths and weakness of TD fNIRS are highlighted, also in comparison with continuous wave (CW) fNIRS. Issues like quantification of the hemodynamic response, penetration depth, depth selectivity, spatial resolution and contrast-to-noise ratio are critically examined, with the help of experimental results performed on phantoms or in vivo. Finally we give an account on the technological developments that would pave the way for a broader use of TD fNIRS in the neuroimaging community.

© 2013 Elsevier Inc. All rights reserved.

Contents

Introduction)	0
Principles of TD fNIRS	0
Basics of NIRS	0
The classical TD NIRS approach	0
The null source detector distance TD NIRS approach	0
TD fNIRS modeling and data analysis	0
Forward model	0
Inverse model	0
Semi-empirical approaches	0
TD fNIRS instrumentation	0
Light sources	0
Detection techniques	0
Delivery and collection system	0
TD fNIRS systems	0
Traditional TD fNIRS systems	0
State-of-the-art TD fNIRS systems	0
Next generation TD fNIRS systems	0
Co-registration with other modalities	0
Performance assessment and standardization	0

Abbreviations: AOTF, acousto-optic tunable filter; CNR, contrast-to-noise ratio; CW, continuous wave; DE, diffusion equation; DTOF, distribution of time-of-flight; FD, frequency domain; FEM, finite element method; fNIRS, functional near-infrared spectroscopy; FWHM, full width at half maximum; GI, graded index; ICCD, intensified charge coupled device; IEC, International Electrotechnical Commission; IRF, instrument response function; ISO, International Organization for Standardization; LDF, laser Doppler flowmetry; MCP, micro-channel plate; MPE, maximum permissible exposure; NA, numerical aperture; NIRS, near-infrared spectroscopy; OD, optical density; OTDR, optical time domain reflectometer; PMT, photomultiplier tube; RTE, radiative transfer equation; SC, supercontinuum; SI, step index; SPAD, single-photon avalanche diode; SRS, space-resolved spectroscopy; TCSPC, time-correlated single photon counting; TD, time domain; TPSF, temporal point spread function.

[☆] Review for Special Issue *Functional Near Infrared Spectroscopy (fNIRS)*, Guest Editors: David Boas, Clare Elwell, Marco Ferrari, Gentaro Taga.

* Corresponding author. Fax: +39 02 2399 6126.

E-mail address: alessandro.torricelli@polimi.it (A. Torricelli).

1053-8119/\$ – see front matter © 2013 Elsevier Inc. All rights reserved.

<http://dx.doi.org/10.1016/j.neuroimage.2013.05.106>

Please cite this article as: Torricelli, A., et al., Time domain functional NIRS imaging for human brain mapping, NeuroImage (2013), <http://dx.doi.org/10.1016/j.neuroimage.2013.05.106>

59	TD fNIRS features	0
60	Quantification	0
61	Penetration depth	0
62	Depth selectivity	0
63	Spatial resolution	0
64	Contrast-to-noise ratio	0
65	Representative in vivo data	0
66	Future perspectives	0
67	Conclusions	0
68	Uncited references	0
69	Acknowledgments	0
70	Appendix A.	0
71	References	0

Q773 Introduction

This review is aimed at presenting the state-of-the-art of time domain (TD) functional near-infrared spectroscopy (fNIRS). As described in a recent review on the history of fNIRS (Ferrari and Quaresima, 2012), while fNIRS dates back about 20 years ago, we have to wait till 1996 for the first single-channel TD fNIRS study to appear in the literature (Obrig et al., 1996), and only some years later, in 1998–2000, the first papers describing multi-channel TD fNIRS instruments were published (Cubeddu et al., 1999; Eda et al., 1999; Hintz et al., 1998; Ntziachristos et al., 1999; Oda et al., 1999; Schmidt et al., 2000). Noticeably, from the physical and technological point of view the origin of TD fNIRS can be traced back to the 1980s, when researchers started exploring the fascinating field of diffusing photons in random (e.g. biological) media (Kuga et al., 1983). A few years later, several studies were focused on diffuse optical imaging and spectroscopy with pulsed laser and photo-detection techniques with picosecond resolution (Chance et al., 1988; Delpy et al., 1988; Ho et al., 1989; Jacques, 1989a, 1989b; Patterson et al., 1989).

Nowadays, about thirty years after the first studies, there is only one dual-channel TD fNIRS commercial system (Hamamatsu Photonics, 2013e) not sold outside of Japan, while there are no commercial TD fNIRS imagers available (Contini et al., 2012; Ferrari and Quaresima, 2012). A few laboratory prototypes have been developed by research groups located in academic or public research centers. To some extent this situation could be interpreted as the failure of the TD approach within biomedical optics. Indeed, in part of the scientific community TD fNIRS (and TD techniques in general) has the reputation of being cumbersome, bulky, and very expensive as compared to commercial continuous wave (CW) fNIRS systems. At the time of writing we cannot ignore all these pitfalls and a gap still exists between CW and TD fNIRS technology. However, we are at the forefront of a new era where recent advances in photonic technologies might allow TD fNIRS to bridge the gap and potentially to overtake CW fNIRS. In this review we try to substantiate this foresight by outlining the key physical and technological aspects that will allow TD fNIRS to reach a maturity stage and to spread in the biomedical and neuroimaging community.

In the following sections we first describe the principles behind TD fNIRS and the basics of TD fNIRS instrumentation. We then highlight the main strengths and weaknesses of TD fNIRS, notably in comparison with CW fNIRS. A concise survey of TD fNIRS data analysis and applications is further reported. Finally we give an account on future perspectives and technological developments that pave the way for a broader use of TD fNIRS in the neuroimaging community.

Principles of TD fNIRS

Basics of NIRS

To properly understand the principles of TD fNIRS it is useful to briefly recall the basics of near-infrared spectroscopy (NIRS). NIRS is

a powerful spectroscopic technique used in several fields (e.g. food and agriculture, chemical industry, life sciences, medical and pharmaceutical, textiles) to nondestructively test samples like liquids (e.g. in the food sector: oil, wine, and milk), powders (e.g. pharmaceutical tablets and pills, and wheat flour), and bulk objects (e.g. in the food sector: fruits and vegetables, meat, and cheese), allowing for their analytical and chemical characterization (Siesler et al., 2002).

In the biomedical field NIRS makes use of light to noninvasively monitor tissue hemodynamics and oxidative metabolism (Ferrari et al., 2012). In the 600–1000 nm spectral range, light attenuation by the main tissue constituents (i.e. water, lipid, and hemoglobin) is in fact relatively low and allows for penetration through several centimeters of tissue. Moreover, the difference in the absorption spectra of oxygenated and deoxygenated hemoglobin allows the separate measurement of the concentration of these two species (O₂Hb and HHb, respectively), and the derivation of physiologically relevant parameters like total hemoglobin concentration (tHb = HHb + O₂Hb) and blood oxygen saturation (SO₂ = O₂Hb / tHb). The term fNIRS is then used to specifically address NIRS applications in the neuroimaging field aiming at mapping and understanding the functioning of the human brain cortex.

In NIRS a weak (a few mW) light signal is injected in the tissue and the emitted signal which carries information on tissue constituents is measured. As a result of the microscopic discontinuities in the refractive index of biological tissues, NIR light is highly scattered, therefore it is the complex interplay between light absorption and light scattering that determines the overall light attenuation. Proper physical models for photon migration (e.g. diffusion, random walk, Monte Carlo) should be used to correctly interpret NIRS signals unraveling the absorption from the diffusive contribution (Durduran et al., 2010; Martelli et al., 2009).

The feature physical quantities in a diffusive medium are the scattering length l_s and the absorption length l_a , representing the photon mean free path between successive scattering and absorption events, respectively. Equivalently, the scattering coefficient $\mu_s = 1 / l_s$ and the absorption coefficient $\mu_a = 1 / l_a$ (typically expressed in units of mm⁻¹ or cm⁻¹) are used to indicate the scattering and the absorption probability per unit length, respectively. Due to anisotropy in light propagation, a reduced scattering coefficient is introduced $\mu_s' = \mu_s (1 - g)$, where g is the anisotropy factor (Martelli et al., 2009).

Typically in a NIRS measurement, light is delivered to and collected from the sample by means of optical fibers (optodes) or other simple optical systems (e.g. relay lenses), which simplify the use of the instrumentation, especially when dealing with clinical measurements on volunteers or patients. A few commercial systems allow placing light sources and detectors directly in contact with the probed tissue. The simplest NIRS measurement configuration is the *transmittance* mode with the injection and collection fibers on opposite surfaces. In the biomedical field this is only possible for a few applications such as hemorrhage detection in newborns (Gibson et al., 2006), thanks to the small size and transparency of the head, optical

169 mammography, where the female breast is gently compressed by
 170 parallel transparent plates (Taroni et al., 2012), or finger arthritis de-
 171 tection (Golovko et al., 2011), where the thinned shape of the finger
 172 makes this possible. On the other hand, the *reflectance* mode exploits
 173 the fact that, thanks to scattering, light is highly diffused in the sam-
 174 ple volume and NIRS measurements become possible with a couple of
 175 optic fibers placed on the same surface of the tissue at a distance of a
 176 few centimeters. A combination of several injection and collection fib-
 177 ers on regularly spaced arrangements permits topography or tomo-
 178 graphic approaches (Selb and Gibson, 2011).

179 Independently from the measurement geometry, three different
 180 NIRS approaches can be implemented: *i*) CW NIRS makes use of a
 181 steady state light source (e.g. a light emitting diode or a laser with in-
 182 tensity constant in time) that can be typically amplitude modulated
 183 at a low (a few kHz) frequency in order to exploit the significant im-
 184 provements in sensitivity available from phase-locked detection tech-
 185 niques, and of a detection apparatus sensitive to light attenuation
 186 changes (e.g. photodiode); *ii*) Frequency domain (FD) NIRS is based
 187 on amplitude modulated light sources (at frequency of the order of
 188 100 MHz or larger, up to ~ 1 GHz) and on the detection of light ampli-
 189 tude demodulation and phase shift; *iii*) TD NIRS employs a pulsed
 190 light source, typically a laser providing light pulses with duration of
 191 a few tens of picoseconds, and a detection apparatus with temporal
 192 resolution in the sub-nanosecond scale. A detailed review of these
 193 different approaches can be found in Wolf et al. (2007).

The classical TD NIRS approach

194

195 TD NIRS relies on the ability to measure the photon distribution of
 196 time-of-flight (DTOF) in a diffusive medium (in the literature the
 197 DTOF is also called temporal point spread function, TPSF). Following
 198 the injection of a light pulse within a turbid medium, the DTOF mea-
 199 sured at a fixed distance from the injection point (typically in the
 200 range of 10–40 mm) is delayed, broadened, and attenuated. The delay
 201 is a consequence of the finite time that light takes to travel the distance
 202 between the source and detector; broadening is mainly due to the
 203 different paths that photons undergo because of multiple scattering;
 204 attenuation appears because absorption reduces the probability of
 205 detecting a photon, and diffusion into other directions within the medi-
 206 um decreases the number of detected photons in the considered direc-
 207 tion. Increasing the source–detector distance yields an increased delay
 208 and broadening of the DTOF and decreases the number of detected pho-
 209 tons. Similar behavior is observed when the scattering increases. Finally,
 210 absorption affects both the signal intensity and the trailing edge (i.e.
 211 slope of the tail) of the DTOF, while leaving the temporal position of
 212 the DTOF substantially unchanged.

213 Fig. 1 shows the effect of source detector distance, absorption, and
 214 reduced scattering on TD NIRS signals in a homogeneous diffusive me-
 215 dium mimicking a biological tissue. While this is an oversimplification
 216 of the real geometry of a human head, nonetheless the model is useful
 217 to present the basics of TD NIRS. In the following section we will discuss

Fig. 1. Principles of TD NIRS. (a) The geometry of TD NIRS measurements in the reflectance mode, The region where photon paths are more likely to occur (the so called “banana shape”) is also schematically depicted; (b) TD NIRS signals at different values of the source detector distance ($\rho = 10\text{--}30$ mm, in steps of 5 mm) for fixed absorption coefficient ($\mu_a = 0.001 \text{ mm}^{-1}$) and reduced scattering coefficient ($\mu_s' = 1.0 \text{ mm}^{-1}$); (c) TD NIRS signals at fixed source detector distance ($\rho = 30$ mm) and fixed reduced scattering coefficient ($\mu_s' = 1.0 \text{ mm}^{-1}$) for different values of the absorption coefficient ($\mu_a = 0.005\text{--}0.025 \text{ mm}^{-1}$ in steps of 0.005 mm^{-1}); (d) TD NIRS signals at fixed source detector distance ($\rho = 30$ mm) and fixed absorption coefficient ($\mu_a = 0.001 \text{ mm}^{-1}$) for different values of the reduced scattering coefficient ($\mu_s' = 0.75\text{--}1.75 \text{ mm}^{-1}$ in steps of 0.5 mm^{-1}).

218 the effect of tissue heterogeneity (e.g. the layered structure of the
219 human head) on TD NIRS signals.

220 *The null source detector distance TD NIRS approach*

221 In 2005 a collaborative effort between the research groups at
222 Politecnico di Milano, Milan, Italy, and at University of Florence,
223 Italy, produced an innovative approach for the investigation of highly
224 diffusive media, based on TD NIRS reflectance measurements at null
225 source–detector separation (Torricelli et al., 2005). The null distance
226 TD NIRS approach was to some extent ground-breaking, since the
227 classical TD NIRS approach to diffuse imaging and spectroscopy
228 fixed source and detector at a large distance to avoid the inaccurate
229 description of light propagation based on photon diffusion at early
230 time and short distance. A major misconception in TD NIRS is that
231 penetration depth is dependent on source detector distance, like in
232 CW NIRS. On the contrary, it was demonstrated by means of numerical
233 simulations that the null distance approach yields better spatial
234 resolution and contrast with respect to the use of longer source detector
235 distances, for an absorbing point-like inclusion embedded in a homogenous
236 medium. The extension to absorption and scattering
237 inclusions with finite dimensions and to layered geometries, better
238 describing some biological structures, such as head or muscle, was
239 reported (Spinelli et al., 2006).

240 **TD fNIRS modeling and data analysis**

241 The raw data in TD fNIRS measurements consist of several time series
242 of DTOFs, acquired at two or more wavelengths, typically from
243 multiple locations. Each DTOF has to be processed to extract the relevant
244 information. Values for the hemodynamic parameters in the brain cortex
245 can be estimated from the corresponding values of the absorption coefficients
246 by means of Beer's law. In a pioneer TD fNIRS study the absorption coefficient
247 was estimated by simply fitting the tail of the measured TD NIRS signal
248 with an exponential law (Chance et al., 1988; Nomura et al., 1997).
249 Nowadays, to properly model light propagation in diffusive media in the TD
250 regime, a wealth of analytical and numerical tools exists, for both simulation
251 purposes (forward model) and for the interpretation of experimental results
252 (inverse model).
253

254 *Forward model*

255 The diffusion equation (DE), an approximation to the radiative
256 transfer equation (RTE) for the case of highly diffusive media, is the
257 most commonly used framework in which photon migration has been
258 treated. A fundamental paper for the TD NIRS approach was published
259 in 1989 by Patterson, Chance and Wilson (Patterson et al., 1989)
260 presenting the analytical solution of the DE for TD NIRS in a homogenous
261 semi-infinite medium or in an infinite slab. Since then, many other papers
262 have been published with improved description of the boundary conditions
263 (e.g. extrapolated or partial current boundary), with analytical solutions
264 for different geometry (e.g. parallelepiped, sphere, cylinder) and for
265 heterogeneous cases (e.g. layered medium, point-like perturbation).
266 It is not the scope of this review paper to describe in details all these
267 contributions. We simply mention for the interested reader that recently,
268 Martelli et al. (2009) have collected in a comprehensive book the basic
269 theory of photon migration together with analytical solutions for the DE
270 in the CW and TD regimes (also implemented in the Fortran programming
271 language) for several geometries. Other handbooks similarly treat the
272 same issues (Hieslcher et al., 2011; Tuchin, 2010).
273

274 Analytical solutions of the RTE have been recently provided for TD
275 NIRS (Liemert and Kienle, 2012; Simon et al., 2013) aiming at overcoming
276 the basic limitation of the DE (e.g. modeling photon migration at very
277 short times or distances, with high absorption, or low

278 scattering). Further, the analytical description of TD perturbation in
279 a homogeneous diffusive medium has greatly improved, being able
280 to deal not only with point-like weakly absorbing inclusions, but
281 also with large highly absorbing objects (Sassaroli et al., 2010).

282 While to a first approximation the description of light propagation
283 in realistic geometries (i.e. adult head) can be treated with simplified
284 analytical models (e.g. layered or perturbed models), it is well known
285 that the use of numerical methods can provide more flexible and accurate
286 solutions. The finite element method (FEM) is a powerful numerical
287 approach to provide solutions of the DE in any geometry and it has
288 been used since 1993 in Biomedical Optics to model light propagation
289 (Arridge et al., 1993). Nowadays freely available tools exist that
290 implement FEM and also handle meshing of MRI anatomical data
291 (NIRFAST, 2013; TOAST, 2013). The Monte Carlo method provides
292 the most accurate description of light propagation in diffusive media
293 (MCML, 2013; Wang et al., 1995), but in the past it was hindered
294 by a very long computational time. Nonetheless it was used by several
295 researchers to properly simulate photon migration in realistic adult and
296 neonatal head models (Boas et al., 2002; Fukui et al., 2003).
297 With the advent of parallelization on graphical processing units
298 (Alerstam et al., 2008b; Fang and Boas, 2009; Ren et al., 2010),
299 computational times have been reduced by up to 100 times, and
300 researchers have revived the use of Monte Carlo methods (Dehaes et
301 al., 2011a; Sassaroli and Martelli, 2012). Recently, a further improvement
302 in terms of speed, memory usage, and accuracy has been obtained
303 by implementing a 3D code that represents a complex domain using
304 a volumetric mesh (Fang, 2010; Fang and Kaeli, 2012).

Inverse model

305
306 The accuracy of non-linear fitting procedures based on the classical
307 Levenberg–Marquardt approach in conjunction with TD NIRS analytical
308 models has been validated several times (Alerstam et al., 2008a;
309 Cubeddu et al., 1996; Spinelli et al., 2009a). Recently, improved
310 fitting procedures based either on the Bayesian approach, also known
311 as optimal estimation (Martelli et al., 2012), or on genetic algorithms
312 (Hieslcher et al., 2000; Zhao et al., 2010) have been proposed.
313 Regularization methods for diffuse optical tomography, largely
314 adopted for processing CW data, have proved to be effective for TD
315 NIRS data (Arridge, 1999; Gao et al., 2004; Selb et al., 2007), as
316 also shown in other fields like optical mammography (Enfield et al.,
317 2007; Intes, 2005) and molecular imaging of small animals
318 (Advanced Research Technologies, 2013; Lapointe et al., 2012).

Semi-empirical approaches

319
320 Semi-empirical phenomenological approaches have been developed
321 aiming at finding quantities derived from measured DTOF that exhibit
322 high sensitivity to deep (cerebral) absorption changes and low
323 sensitivity to superficial (systemic) absorption changes. Two main
324 approaches have been pursued: the first involves the calculation of
325 the moments of the DTOF, focusing in particular on the second order
326 moment (i.e. variance) (Liebert et al., 2004, 2012), or on higher
327 order moments (Hervé et al., 2012); an alternative approach exploits
328 time gating of the DTOF to separate late (deep) and early (superficial)
329 photons (Contini et al., 2007; Selb et al., 2005). The main advantage
330 of these methods is that they do not rely on nonlinear fitting procedures,
331 rather they are based on linear direct formulas, significantly increasing
332 the contrast-to-noise ratio.

333 Fig. 2 shows an experimental DTOF and the instrument response function
334 (IRF) obtained by facing the injection and collection fiber. Moments of
335 the DTOF and a typical time window used in the time-gating semi-
336 empirical approach are also shown. Data were acquired by the system
337 described in Contini et al. (2006).

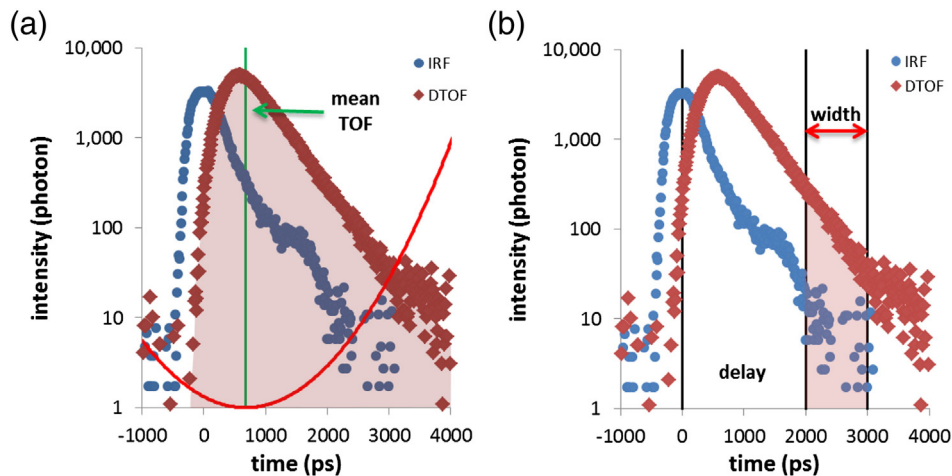


Fig. 2. Typical TD NIRS signal. Experimental DTOF (red diamonds) and corresponding IRF (blue diamonds), measured by the system described in Contini et al. (2006). An example of a time window (delay = 2000 ps; width = 1000 ps) used in the time-gating semi-empirical approach is also shown.

338 TD fNIRS instrumentation

339 The values of the optical parameters of biological tissue (i.e.
 340 human head) in the visible and NIR spectral range (e.g. $\mu_a =$
 341 $0.005\text{--}0.05\text{ mm}^{-1}$; $\mu_s' = 0.5\text{--}2.5\text{ mm}^{-1}$) (Torricelli et al., 2001), to-
 342 gether with the values of source detector distances commonly used
 343 (10–30 mm), set the time scale of TD NIRS measurements in the
 344 range of 0.1–10 ns, and fix the light attenuation level to about 8 opti-
 345 cal densities. Therefore, the crucial features in the designing of a TD
 346 fNIRS system are temporal resolution and sensitivity. It is therefore
 347 the combination of a specific light source with a proper detection
 348 technique that determines the overall performances of a TD NIRS
 349 (and TD fNIRS) set-up. A further element that can influence the func-
 350 tioning of the TD NIRS set-up is the delivery and collection system
 351 used to bring light pulses to the measured sample and to collect
 352 the NIRS signal. We briefly illustrate the main aspects related to
 353 these building blocks, before presenting the existing TD fNIRS
 354 systems.

355 Light sources

356 Current commercially available pulsed lasers produce short (10–
 357 100 ps) and ultra-short (10–100 fs) light pulses, with repetition
 358 frequency up to 100 MHz, and average power in the range of 1–
 359 1000 mW.

360 Solid state lasers (e.g. Ti:Sapphire) provide a powerful and flexible
 361 solution for laboratory set-ups (Coherent Inc., 2013; Newport
 362 Corporation, 2013). They can in fact offer average power of ~ 1 W, rep-
 363 etition rates < 100 MHz, and pulse duration under 1 ps over a broad
 364 wavelength range (e.g. 750–850 nm). They provide the advantages of
 365 wavelength tunability over 400 nm, and high output power enabling
 366 time-multiplexing of the source over multiple positions. Their use in clin-
 367 ical TD fNIRS devices is somehow limited, mainly due to a bulky case and
 368 to the long time (~ 10 s) required to switch between wavelengths.

369 Pulsed diode lasers are provided by several companies (Advanced
 370 Laser Diode Systems GmbH, 2013; Alphalas GmbH, 2013; Becker &
 371 Hickl GmbH, 2013a; Edinburgh Photonics, 2013; Hamamatsu
 372 Photonics, 2013d; PicoQuant GmbH, 2013b). They are compact and
 373 robust, and they typically come with sufficient average power
 374 (< 5 mW), narrow spectral bandwidth (< 10 nm) and pulse duration
 375 (< 500 ps). Several TD systems have adopted this type of light source
 376 (see Tables 1 and 2). Indeed, to reach acceptable performances, there
 377 is always a trade-off between output power and pulse duration: due
 378 to the particular modulation strategy (gain switching), output
 379 power < 1 mW has to be selected to obtain pulse duration < 100 ps.

Another drawback is a long warm-up time (in some cases > 60 min)
 needed to achieve pulse time stability in the picosecond range.

In the last years, a few companies (Fianium UK Ltd., 2013b; NKT
 Photonics A/S, 2013b) have delivered commercial high-power fiber las-
 ers based on supercontinuum (SC) generation. These devices are
 ultra-broadband radiation sources with high spectral brightness and ex-
 cellent beam quality. Typically, a total average power of < 10 W is gener-
 ated over a broad spectral range (e.g. 400–2000 nm), allowing average
 spectral power of 1 mW/nm. A series of optoelectronic accessories are
 used for automatic wavelength selection and power adjustment. Only
 preliminary TD fNIRS studies have been reported with these sources,
 yet they could potentially replace laser diodes in clinical systems. For
 this to happen, issues related to power stability (critical due to the
 nonlinear SC generation) and robustness (affected by the durability of fu-
 sion and splicing in the photonic crystal fiber) have to be solved (e.g. by
 means of feedback loop and opto-mechanical solutions).

We have to notice that the laser power should be fixed to proper
 values in order to avoid possible damage or injury to the tissue. No
 maximum permissible exposure (MPE) value for the brain has been
 determined, however, the light intensity on the brain surface during
 fNIRS can be safely estimated to be only a few percent of the solar ir-
 radiation (Kiguchi et al., 2007). Despite the fact that these consider-
 ations were made for CW fNIRS, they hold also for TD fNIRS. Ac-
 cording to the safety regulations (International Electrotechnical
 Commission, 2001) the criteria for the MPE assessment in the case
 of a repetitively pulsed or modulated lasers are: i) each single pulse
 of the train shall not exceed the MPE for a single laser pulse of the
 same duration; ii) the average exposure for a pulse train of duration
 T shall not exceed the MPE for a single pulse of duration T; iii) the av-
 erage exposure for a pulse train shall not exceed the MPE for a single
 pulse multiplied by the correction factor $N^{-0.25}$ (where N is the total
 number of pulses impinging the tissue). The first criterion limits the
 energy of a single pulse in order to avoid nonlinear effects that can
 damage the tissue; in this case pulse duration and peak power are
 critical. The second and third criteria limit the average exposure in
 which the key factor is the average power. Thus, in cases in which a
 single pulse does not have sufficient energy to cause damage, and
 considering a repetition frequency of tens of MHz, the limiting factor
 is the average power of the laser, as for CW laser light.

Detection techniques

To detect weak and fast light signals, several detection techniques
 with temporal resolution in the range of 1–250 ps and sufficient sen-
 sitivity are available.

Table 1

Traditional TD fNIRS systems.

Group	Light source	Wavelength (nm)	Average power (mW)	Repetition rate (MHz)	Detection technique	Count rate (MHz)	IRF FWHM (ps)	Source channels	Detection channels	Reference
Physikalisch-Technische Bundesanstalt Berlin, Germany	Ti:Sapphire	775, 805, 835 (serial)	800 (?)	80 (?)	TCSPC	NA	35	1	1	Obrig et al. (1996)
Stanford University Palo Alto, California	Laser diode	785, 850	0.1	NA	OTDR	NA	NA	34 (serial)	34	Hintz et al. (1998)
Shimadzu Corporation, Hamamatsu Photonics, Ministry of Int. Trade and Industry, Hokkaido University Japan	Laser diode	761, 791, 830	0.25	5	TCSPC	1	150		64	Eda et al. (1999)
Politecnico di Milano Milan, Italy	Laser diode	672, 818	1	80	TCSPC	1	200	4	4	Cubeddu et al. (1999)
University of Pennsylvania, Philadelphia, Pennsylvania	Laser diode	780, 830	0.020	5	TCSPC	4	50	9	8	Ntziachristos et al. (1999)
TRS-10, Hamamatsu Photonics Japan	Laser diode	759, 797, 833	<0.1	5	TCSPC	<1	150	1	1	Oda et al. (1999) Ohmae et al. (2007)
University College London London, United Kingdom	Ti:Sapphire/fiber laser	800 780, 815	800 > 50	80 40	TCSPC	0.3	80–150	32 (serial)	32	Gibson et al. (2006) Schmidt et al. (2000)
TRS-16, Hamamatsu Photonics Japan	Laser diode	760, 800, 830	1	5	TCSPC	<4	500	8 (serial)	16	Yamashita et al. (2003)
Physikalisch-Technische Bundesanstalt Berlin, Germany	Laser diode	687, 803, 826	0.5	20	TCSPC	1	600	1	4	Liebert et al. (2004)
Politecnico di Milano Milan, Italy	Laser diode	685, 780	1	80	TCSPC	4	200	2	8	Torricelli et al. (2004)
Institut de Physique Biologique Strasbourg, France	Laser diode	690, 785, 830, 870	1	20	TCSPC	8	200	1	8	Montcel et al. (2004) Montcel et al. (2005)
Martinos Center for Biomedical Imaging, Boston	Ti:Sapphire	One wavelength tuned in the range of 750 to 850 nm	1000	80	Time-gated ICCD	NA	500	32 (serial)	18	Selb et al. (2005) Selb et al. (2006)

Non-linear optical-gating (by means of Kerr effect, parametric amplification, or non-linear up-conversion) can be used if time-gating of the optical signal in the sub-picosecond time scale is required (Tolguenec et al., 1997; Wang et al., 1991). Indeed this approach requires complex and bulky system set-ups that limit its use to the laboratory scale and in particular for those applications where extreme time resolution is really needed: in the biomedical field the molecular imaging of small animals by optical projection tomography (Bassi et al., 2010), or in the physics of matter field the characterization of photonic glasses (Toninelli et al., 2008). On the contrary, in fNIRS

applications sub-picosecond time resolution is definitely not mandatory (see also next section Temporal resolution).

The streak camera is a detection apparatus with time resolution in the 1–10 ps range able to operate as multi-wavelength or multi-channel detector by exploiting its bi-dimensional design (Hamamatsu Photonics, 2013a). TD fNIRS experiments in small animals were recently reported with a streak camera apparatus (Mottin et al., 2011; Vignal et al., 2008), but no extension to human studies seems feasible due to a very high cost (also compared to non-linear time gating) and an overall complexity that prevents the use by personnel without an adequate expertise in

Table 2

State-of-the-art TD fNIRS systems.

Group	Light source	Wavelength (nm)	Average power (mW)	Repetition rate (MHz)	Detection technique	Count rate (MHz)	IRF FWHM (ps)	Source channels	Detection channels	Reference
TRS-20, Hamamatsu Photonics Japan	Laser diode	760, 800, 830	0.25	5	TCSPC	1	250	2	2	Oda et al. (2009)
Physikalisch-Technische Bundesanstalt Berlin, Germany	Laser diode	689, 797, 828	1	42	TCSPC	2	750	9 (serial)	4	Wabnitz et al. (2005) Wabnitz et al. (2010)
Politecnico di Milano Milan, Italy	Laser diode	690, 830	1	80	TCSPC	8	500	16 (serial)	16	Contini et al. (2006) Contini et al. (2009)
Politecnico di Milano Milan, Italy	Laser diode	690, 830	1	80	TCSPC	4	500	2	2	Re et al. (2010)
Institute of Biocybernetics and Biomedical Engineering Warsaw, Poland	Laser diode	687, 832	1	80	TCSPC	16	<800	18 (serial)	8	Kacprzak et al. (2007)

controlling of scientific instrumentation. Pioneer fNIRS studies were performed to determine the optical path-length in the adult and/or newborn head (Delpy et al., 1988; Ferrari et al., 1993; van der Zee et al., 1992; Wyatt et al., 1990). No further fNIRS studies on human have been reported to our knowledge.

The pioneer studies by Hintz et al. (1998) and Benaron et al. (2000) used a TD fNIRS system based on a modified optical time domain reflectometer (OTDR). This approach has been later abandoned because of poor performances.

The time-correlated single photon counting (TCSPC) technique (O'Connor and Phillips, 1984) has been extensively used for fluorescence lifetime measurements since the 1970s and later for TD NIRS measurements in diffusive media. In a TCSPC experiment, the temporal profile of the NIRS signal is not directly measured but is retrieved by repeatedly measuring the delay between the trigger of the injected laser pulse and the detection of a (diffusively) reemitted photon for a statistically significant number of photons. A detector with a fast (<1 ns) and stable single electron response is required. A variety of such detectors are commercially available: photomultiplier tube (PMT) (Hamamatsu Photonics, 2013c), micro-channel plate (MCP) PMT (Hamamatsu Photonics, 2013b), hybrid detector (Becker & Hickl GmbH, 2013b; PicoQuant GmbH, 2013a), and single-photon avalanche diode (SPAD) (Excelitas Technologies Corp, 2013; ID Quantique SA, 2013; Micro Photon Devices, 2013a; PicoQuant GmbH, 2013e; SensL, 2013b). A key parameter in TCSPC is the count rate, i.e. the number of photons per second which can be processed (or simply counted) without exceeding the single photon statistics. In the 1980s light sources were characterized by low intensity and low repetition rate (<10 kHz), and TCSPC electronic circuit speed was also limited (the dead time after the detection of a photon was on the order of 10 μ s). The consequence for TCSPC was a very low count rate (<10⁴ photon/s), which resulted in long acquisition times (several minutes). Nowadays the speed of commercially available TCSPC modules is 1000 times faster than the classic TCSPC devices (e.g. the dead time is as low as 100 ns). In combination with a laser with repetition rate in the order of tens of MHz, a TCSPC module has potentially the capability of processing a few 10⁶ photons/s. Further, multi-dimensional TCSPC allows the simultaneous recording of photons from a large number of detectors (Becker & Hickl GmbH, 2013d; PicoQuant GmbH, 2013d; SensL, 2013a). A complete and updated description of TCSPC systems and applications (including TD fNIRS) can be found in Becker (2005).

Detection of TD NIRS signal is also possible with a time-gated intensified charge coupled device (ICCD) camera. It basically consists of a photocathode, an MCP PMT, and a phosphor screen. High temporal resolution can be achieved by fast gating of the intensifier cathode of the ICCD camera (LaVision BioTec GmbH, 2013). Years ago the time resolution was limited to about 1 ns restricting the use of the time-gated ICCD camera, while recently ultra-short gates (e.g. <100 ps) can be achieved by using smaller image tubes. Like TCSPC, a time-gated ICCD camera is characterized by sensitivity down to single photon detection. Like a streak camera, the time-gated ICCD system is a bi-dimensional device, thus potentially able to measure the spatial and temporal profile of the remitted light from a diffusive medium by acquiring different images synchronized for different time delays with respect to the injection of the laser pulse. Every image contains the spatial information at a certain time instant, while the successive values stored in the memory and referring to the same pixel determine the temporal distribution of the detected signal. TD NIRS setups based on a time-gated ICCD camera have been reported for optical imaging of diffusive phantoms (D'Andrea et al., 2003) or small animals (Niedre et al., 2006). Preliminary TD fNIRS studies have used the time-gated ICCD camera as multi-channel device in combination with optical fibers of different lengths allowing for simultaneous detection of several time-gates (Selb et al., 2005, 2006), or as an imaging device (Sawosz et al., 2010; Zhao et al., 2011).

Nowadays, TCSPC systems are more easily found in prototypes and instruments for TD fNIRS (see also next section TD fNIRS systems). Since there is no striking advantage of TCSPC over time-gated ICCD camera, the choice of the technique is rather determined by an overall balance between costs, complexity and performances in relation also to the specific applications.

When the TD null source detector distance approach is considered, several technological issues should be taken into account. The most severe obstacle is the presence of early photons. With decreasing source detector distance, early photons increase at a much faster pace than the late photons and saturate the detection electronics. This prevents the extraction of long-lived photons that carry information from deep structures. Thus, an efficient mechanism to gate, or at least to reduce, the early photons is needed to be able to exploit the advantages of this approach.

This modality is available for a MCP PMT by acting on its gain, for an ICCD camera by operating on the gain of the intensifier, and also for a streak camera by controlling the ramp voltage so as to sweep electrons corresponding to initial photons out of the active surface of the CCD detector. In practice, in all these devices, only the detection stage after the photocathode is altered. Therefore this solution is effective if the required extinction ratio is not severe, since initial photons still impinge onto the photocathode and extract electrons, causing damage to the active surface and increasing significantly the background noise. An attempt to obtain null distance TD NIRS with an ICCD based system has been reported (Sawosz et al., 2012).

A possible alternative is the use of a SPAD. A key difference of SPAD detectors with respect to other approaches is the possibility to enable the device above threshold very quickly. When the SPAD is disabled, the avalanche process cannot start, and most of the electron-hole pairs generated by the incoming photons recombine within the active area in a few tens of ps. Thus, this device is not damaged by the burst of initial photons, and a strong rejection of early photons can be achieved.

The first demonstration of the null distance approach with a SPAD based system has been reported by the research group at Politecnico di Milano, Milan, Italy (Pifferi et al., 2008).

Finally, we mention that a completely different method for measuring TD optical quantities has been proposed using pseudorandom bit sequences as light source and a cross-correlation scheme to retrieve the impulse response (Chen and Zhu, 2002, 2003). While, the overall performances of this approach were not satisfactory, this is an interesting example of cross-contamination between different fields.

Delivery and collection system

Due to the limitations related to the size of TD NIRS light sources and detectors, it is typically required that the light pulses are delivered to the sample (e.g. the head) and conveyed to the detectors by some kind of optical system. The easiest, and most common way, is to couple light into optical fibers or bundles, which has the additional advantage, from the point of view of safety, of electrically isolating the measurement site from the device.

Single mode optical fibers are characterized by small core diameter (<10 μ m) and typically operate in a narrow spectral range (<100 nm) centered at a specific operating wavelength in the visible and NIR range. Multimode optical fibers are built with core diameter of different sizes (10–1000 μ m) and operate over a broad spectral range (from ultraviolet to NIR). Attenuation, numerical aperture (NA), and dispersion are the main characteristics related to optical fibers that have to be considered when designing a TD fNIRS system.

Light attenuation in modern low hydroxyl ions fused silica optical fibers (used in long range data transmission) is below 10 dB/km, while plastic optical fibers (for short range data transmission) have higher attenuation (<100 dB/km) (Gowar, 1993). Attenuation is

572 therefore negligible for fiber length in the order of 10 m, as used in
573 fNIRS.

574 The NA is related to the maximum acceptance angle of an optical
575 fiber and it influences the light gathering ability of the fiber (Gowar,
576 1993). To maximize collection efficiency in TD NIRS, high NA values
577 (e.g. >0.3) and large core diameters (e.g. >500 μm) should be pre-
578 ferred for the collection fibers since the total power that can be collected
579 from a diffusive sample by a fiber scales with the squares of the NA and
580 of the radius. Multimode fibers have to be preferred to single mode fi-
581 bers to optimize light transmission efficiency in the TD fNIRS system.

582 Dispersion is a crucial parameter for TD fNIRS since it broadens the
583 light pulses traveling in the fiber. When using a narrow bandwidth
584 source (e.g. laser), total dispersion is dominated by modal dispersion
585 in a multimode fiber, while material (chromatic) dispersion can be
586 dominant in a single mode fiber. Modal dispersion can be greatly re-
587 duced by a proper design of the refraction index profile of the optical
588 fiber: graded index (GI) fibers should be preferred to step index (SI) fi-
589 bers. Typical value of dispersion in GI fibers is 1 ps/m, while it increases
590 to about 100 ps/m in SI fibers (Gowar, 1993).

591 The optimal solution to reduce pulse broadening and maximize light
592 transmission for light delivery and collection would be a multimode GI
593 optical fiber with the highest NA and the largest core diameter.
594 Multimode GI optical fibers are typically fabricated with 50, 62.5 and
595 100 μm core diameters, therefore limiting their applications in TD
596 fNIRS to light delivery. For maximizing TD signal collection from the tis-
597 sue a fiber with a much larger diameter is required. Unavoidably, SI fibers
598 have to be chosen, being commercially available with core diameter up
599 to 3000 μm. Unfortunately, the bending radius of such large fibers is
600 not negligible (e.g. >50/>150 mm for momentary/long term bend of a
601 1000 μm core diameter fiber), resulting in a limited flexibility. For ease
602 of use, especially in the clinical environment, fiber bundles, made by
603 gathering hundreds of smaller flexible fibers, have to be preferred.
604 Modal dispersion turns out to be a limiting factor since SI fibers are
605 used (the use of GI fibers would not improve the performances due to
606 waveguide dispersion effects). A trade-off between fiber bundle length
607 and NA is required, typically obtained by limiting fiber bundle length
608 to a couple of meters. The use of longer bundles determines an overall
609 unacceptable temporal resolution, quantified by the full width at half
610 maximum (FWHM) of the IRF. Values of the IRF larger than 1 ns compro-
611 mise the accuracy of TD NIRS measurements (Liebert et al., 2003).

612 Additional components and devices are typically used in delivery
613 and collection systems. Switches, splitters and galvo mirrors multiplex
614 light pulses in different locations of the sample (e.g. for mapping pur-
615 poses). Variable neutral density attenuators are used to equalize the
616 signals, while lenses help in focusing light to the detection systems.
617 Band-pass filters prevent room light to interfere with the TD NIRS sig-
618 nal, and help in collecting the fluorescence signal from endogenous or
619 exogenous chromophores like indo-cyanine green (Gerega et al.,
620 2012; Milej et al., 2012). The main effect of these components is the in-
621 troduction of additional attenuation terms that could reduce the overall
622 responsivity of the TD fNIRS set-up (Wabnitz et al., 2011), while they
623 have a negligible effect on the IRF.

624 **TD fNIRS systems**

625 In this section we present a survey of traditional (Table 1),
626 state-of-the-art (Table 2) and next generation (Table 3) TD fNIRS sys-
627 tems. With the term *traditional* we refer to TD fNIRS systems that, to
628 our knowledge, have been now discontinued, or replaced by novel
629 upgraded systems, or used for other applications. It is worth noting
630 that most of these systems represented a breakthrough as compared
631 to classical TD NIRS laboratory systems, typically based on bulky gas la-
632 sers and massive accessories. Indeed, they were compact at the level of
633 being transportable out of the lab (see Fig. 3). In most cases they were
634 able to operate simultaneously at two or more wavelengths. Parallel ac-
635 quisition of up to tens of channels was possible, opening the way to

Table 3
Next generation TD fNIRS systems.

Group	Light source	Wavelength (nm)	Average power (mW)	Repetition rate (MHz)	Detection technique	Count rate (MHz)	IRF FWHM (ps)	Source channels	Detection channels	Reference
University College London, United Kingdom	SC fiber laser	Up to 8 selected in the 650–825 nm spectral range	<2.5	40	TCSPC	8	220	32 (serial)	32	Hebden et al. (2012a)
MONSTIR2	SC fiber laser	Up to 6 selected in the 680–840 nm spectral range	<100	60	Time-gated ICCD	NA	500	16 (serial)	25	Hebden et al. (2012b)
Martinos Center for Biomedical Imaging, Boston	Laser diode	690, 830	1	80	TCSPC	16	400	16 (serial)	8	Selb and Boas (2012)
Politecnico di Milano Milan, Italy	Laser diode	705, 830	<5	40	TCSPC	2	750	10	4	Selb et al. (2013)
foXYZ	SC fiber laser	690	1	20	TCSPC	2	<100	1 (scanning)	1 (scanning)	Contini et al. (2013b)
Physikalisches-Technische Bundesanstalt Berlin, Germany	SC fiber laser	710, 820	<100	40	TCSPC Fast gated	2	100	1	1	Steinkellner et al. (2012)
Physikalisches-Technische Bundesanstalt Berlin, Germany	SC fiber laser	780	<3	50	TCSPC (TDC)	16	<300	2 (scanning)	32 × 32	Mazurenka et al. (2012)
Confocal null distance Politecnico di Milano Milan, Italy	Laser diode	780	<3	50	TCSPC (TDC)	16	<300	2 (scanning)	32 × 32	Mazurenka et al. (2013)
Null distance Ecole Polytechnique Federale de Lausanne and University Hospital Zurich	Laser diode	780	<3	50	TCSPC (TDC)	16	<300	2 (scanning)	32 × 32	Contini et al. (2013a)
3D SPAD imager	Laser diode	780	<3	50	TCSPC (TDC)	16	<300	2 (scanning)	32 × 32	Mata Pavia et al. (2011a)
										Mata Pavia et al. (2011b)

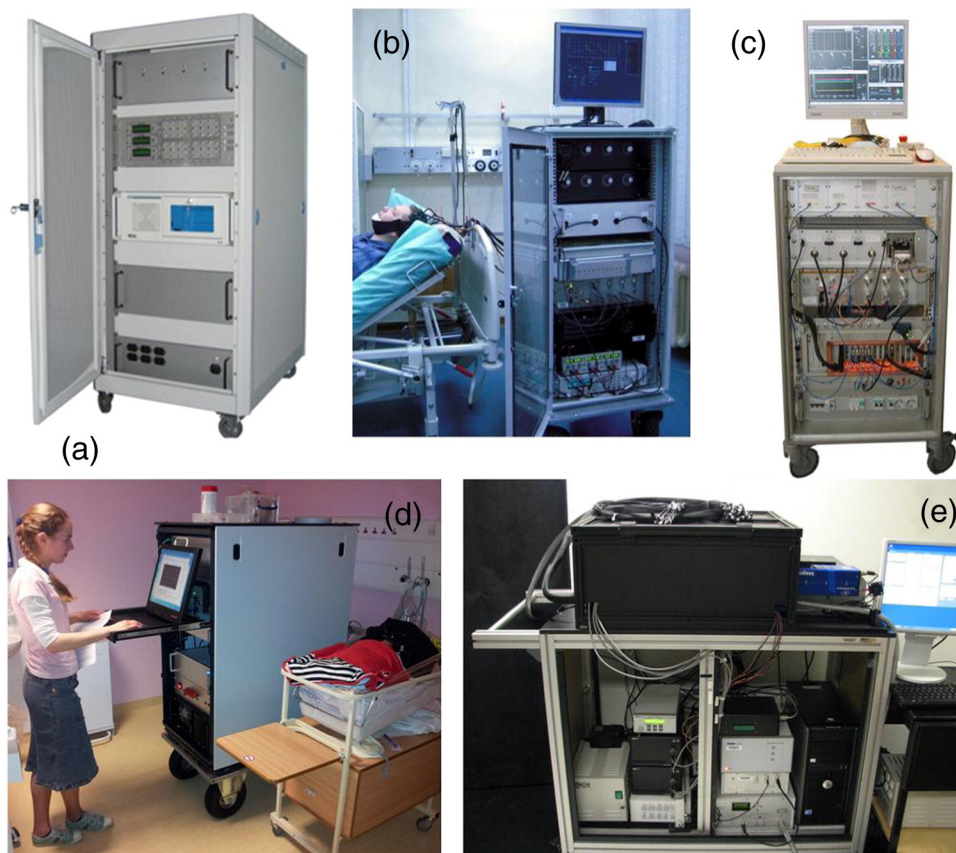


Fig. 3. Photos of TD fNIRS devices. (a) The fOXY medical device developed at Politecnico di Milano, Milan Italy (Contini et al., 2006, 2009); (b) the brain imager developed at the Institute of Biocybernetics and Biomedical Engineering, Warsaw, Poland (Kacprzak et al., 2007); (c) the brain imager developed at Physikalisch-Technische Bundesanstalt, Berlin, Germany (Wabnitz et al., 2005, 2010); (d) the MONSTIR2 developed at the Department of Medical Physics and Bioengineering, University College London, United Kingdom (Hebden et al., 2012a, 2012b); (e) the TGI-2 imager developed at Massachusetts General Hospital, Athinoula A. Martinos Center, Charlestown, Massachusetts (Selb and Boas, 2012; Selb et al., 2013).

mapping experiments. Nonetheless, they were characterized by sub-optimal performances due to a reduced count rate (on average <1 MHz) and to low average power (<1 mW) of the light sources. In many cases they were used for static imaging with very long acquisition times (up to several minutes), or for monitoring hemodynamic changes in a few channels with a relatively short acquisition time (<1 s).

We consider then the *state-of-the-art* TD fNIRS systems that in the last five years (2008–2012) have been used for research and clinical fNIRS studies in adults and neonates, as reported in the literature.

Finally we report on the *next generation* TD systems to present the work that, to our knowledge, researchers are carrying out to test novel approaches and to implement advanced technological solutions aiming at improving performances of TD fNIRS devices. These set-ups have only provided proof of principle results, while no clinical studies have been reported.

We conclude this section reporting on the issues related to multimodality co-registration of TD fNIRS with other techniques and to performance assessment and standardization of TD fNIRS system.

Traditional TD fNIRS systems

A collaborative effort among the research groups at the Department of Physics, Department of Bioengineering, and Department of Biochemistry/Biophysics at University of Pennsylvania, under the coordination of Prof. Britton Chance, developed a multi-channel TD instrument (Ntzachristos et al., 1999). Spatially resolved measurements of contralateral primary motor-cortex activation during voluntary finger tapping were performed and successfully coregistered with fMRI data. Results

demonstrated the efficiency of the device in the detection of local optical variations as well as its good performances in coregistration with fMRI.

The TD fNIRS system developed at Stanford University, Palo Alto, California, was characterized by a large number of channels (34×34), allowing for the first diffuse optical tomography measurements, but it suffered for very low sensitivity. The acquisition times were tremendously long and applications were limited to static imaging of hemorrhage in newborns (Benaron et al., 2000).

The tomographic TD fNIRS system developed by the research group at the Department of Medical Physics and Bioengineering, University College London, overcame most of the limitations of the previous system, and it was successfully used not only for quasi static imaging in diseased newborns (Austin et al., 2006; Hebden et al., 2004) but also for functional studies in healthy newborns (Gibson et al., 2006).

After a preliminary TD fNIRS study with a laboratory set-up (Obrig et al., 1996), the research group at Physikalisch-Technische Bundesanstalt in Berlin, Germany, developed a compact system that was used for very relevant studies in which it was first demonstrated the ability of the TD approach to discriminate intra-cerebral and extra-cerebral contribution (Liebert et al., 2004; Steinbrink et al., 2001).

The compact 8-channel TD fNIRS system developed at Politecnico di Milano, Milan, Italy was used for studying the bilateral prefrontal cortex hemodynamic response to a verbal fluency task (Quaresima et al., 2005).

The research group in Strasbourg used an eight-channel system based on picosecond laser sources and a multi-anode MCP PMT to perform a single point measurement during a finger tapping experiment

(Montcel et al., 2005, 2006). An upgraded version of this system is now being used for molecular imaging of small animals (Montcel and Poulet, 2006).

Several studies on piglets (Ijichi et al., 2005a), infants (Ijichi et al., 2005b, 2005c) and adult (Hoshi et al., 2006; Kakihana et al., 2010, 2012; Ohmae et al., 2006, 2007; Sato et al., 2007; Yokose et al., 2010) have been reported with the commercial TD fNIRS instrument TRS-10 developed by Hamamatsu Photonics. Fewer studies were performed with the modified multi-channel set-up (Oda et al., 1999; Ueda et al., 2005).

The research group at the Massachusetts General Hospital, Athinoula A. Martinos Center, Charlestown, Massachusetts, developed a TD fNIRS system based on an ICCD detector coupled to 18 optical fibers of 7 different lengths creating an optical delay, and enabling simultaneous detection in 7 windows by step of 500 ps. Preliminary single wavelength results on adults performing a motor task were reported (Selb et al., 2005, 2006).

State-of-the-art TD fNIRS systems

Nowadays, there is only one commercial TD fNIRS system, the TRS-20 developed in Japan by Hamamatsu Photonics and sold (only in Japan) as an investigational-use only, stand-alone two-channel system. The TRS-20 employs thermo-electrically controlled picosecond laser diodes, operating at 760 nm, 800 nm, and 830 nm, with an overall temporal resolution < 150 ps (IRF FWHM), and proprietary fast photomultipliers and TCSPC module (Hamamatsu Photonics, 2013e; Oda et al., 2009).

Existing TD fNIRS systems with clinical applications have been mainly developed by European research groups located in academic or public research centers.

The research group at Physikalisch-Technische Bundesanstalt, Berlin, Germany, has developed a three-wavelength four-detection-channel TCSPC instrument (Wabnitz et al., 2005, 2010) that has been effectively used for bedside assessment of cerebral perfusion in stroke patients (Liebert et al., 2005; Steinkellner et al., 2010), to explore neurovascular coupling in combination with magneto-encephalography (Mackert et al., 2008; Sander et al., 2007) and to study systemic artifacts in TD fNIRS (Kirilina et al., 2012). With little modifications in the light sources and in the detectors, the system has been also used for fluorescence detection from exogenous chromophores in the adult human brain (Jelzow et al., 2012; Liebert et al., 2006).

In Warsaw, Poland, a 32-channel configuration has been assembled by doubling the switching and detection elements at the Institute of Biocybernetics and Biomedical Engineering (Kacprzak et al., 2007) and used in clinical applications such as brain oxygenation measurements during carotid endarterectomy (Kacprzak et al., 2012) and detection of brain traumatic lesions (Liebert et al., 2011).

A 16-source and 16-detector TD fNIRS imager with fast acquisition time (> 5 ms per channel) was developed at Politecnico di Milano, Milan, Italy (Contini et al., 2006; Contini et al., 2009) and used to map the cortical response in healthy volunteers during cognitive studies (Butti et al., 2009; Molteni et al., 2012) and in epileptic patients with movement disorders during motor tasks (Torricelli et al., 2011). The same group developed a 2-source and 2-detector TD fNIRS system based on the space-multiplexing approach (Re et al., 2010) with improved sensitivity that was used to investigate the sensitivity of TD fNIRS to cortical and superficial systemic response (Aletti et al., 2012).

Finally, we mention that a couple of European companies sell components (pulsed lasers, photo-detectors and TCSPC modules) and stand-alone TD systems, with up to 4 channels, mainly for standard fluorescence lifetime applications, single molecule spectroscopy, and lifetime imaging with scanning microscopes (Becker & Hickl GmbH, 2013c; PicoQuant GmbH, 2013d). These products could be properly adapted to be used for investigational TD fNIRS studies (Diop et al., 2010).

Next generation TD fNIRS systems

The research group at the Department of Medical Physics and Bio-engineering, University College London, designed and developed an upgraded version of the tomographic TD fNIRS system (MONSTIR 2). Main improvements with respect to the previous device are the use of a SC fiber laser equipped with an acousto-optic tunable filter (AOTF) device allowing a multi-wavelength approach, and the use of modern TCSPC acquisition boards to replace the obsolete electronic modules. The system has been tested on preliminary measurements on newborns (Hebden, 2012a; Hebden et al., 2012b).

The ICCD based TD fNIRS system developed at the Massachusetts General Hospital, Athinoula A. Martinos Center, Charlestown, Massachusetts, has been recently upgraded by introducing a SC fiber laser to replace the Ti:Sapphire laser, and a set of band-pass filters on a fast filter wheel to properly and rapidly select the operating wavelengths (Selb and Boas, 2012; Selb et al., 2013). The main limitation of the previous set-up (i.e. the operation at a single wavelength) has been therefore overcome.

A novel TD fNIRS system has been recently developed by researchers at Politecnico di Milano, Milan, Italy. The use of hybrid PMT with reduced afterpulsing allows acquisition of TD fNIRS signals over a larger dynamic and temporal range. Further, the space-multiplexing approach implemented by means of a cascade of fast fiber optic switches that sequentially delivers the different wavelengths in different injection channels, eliminates the cross-talk between TD NIRS signal at different wavelengths (Contini et al., 2013b).

The research group at Physikalisch-Technische Bundesanstalt, Berlin, Germany has been testing novel approaches for light delivery and collection. A cascade of splitters is used to illuminate in parallel several injection points to potentially reduce power loss. Time-multiplexing of TD NIRS signal from different channels allows parallel detections. Moreover, advanced PMT with improved sensitivity in the NIR (e.g. GaAs surface) or reduced after-pulsing (e.g. hybrid PMT) has been tested (Steinkellner et al., 2012).

In a different set-up, a novel non-contact system is used that utilizes a quasi-null source detector separation approach for TD NIRS, taking advantage of polarization-sensitive detection and a state-of-the-art fast-gated SPAD to detect late photons only, bearing information about deeper layers of the biological tissue. Measurements on phantoms and preliminary in vivo tests demonstrate the feasibility of the non-contact approach for the detection of optically absorbing perturbations buried up to a few centimeters beneath the surface of a tissue-like turbid medium (Mazurenka et al., 2012, 2013).

On the basis of the experience gained with advanced laboratory setups (Pifferi et al., 2008; Tosi et al., 2011), a next generation TD fNIRS prototype implementing the null distance approach has been recently designed and developed at Politecnico di Milano, Milan, Italy. The instrument is based on a custom developed SC fiber laser (Fianium Ltd., Southampton, United Kingdom), providing two independent outputs at 710 nm and 820 nm, with a repetition frequency of 40 MHz, 100 mW average power at each wavelength, and a FWHM of < 50 ps. A fast-gating (< 500 ps) front-end electronics and two SPAD detectors are used to simultaneously acquire photons at different time-windows. Preliminary in vivo results show, for the first time, the possibility to non-invasively monitor cortical O₂Hb and HHb changes during a motor task with a source detector distance of < 5 mm (Contini et al., 2013a).

The collaboration between Ecole Polytechnique Federale de Lausanne and University Hospital Zurich, Switzerland, allowed researchers to design a 3D imager based on SPAD imager with 128 × 128 pixels capable of performing TD NIRS measurements with a resolution of < 100 ps. The system is equipped with picosecond pulsed diode laser and a telecentric objective for non-contact measurements. The main drawback is at present the long time required to the readout circuitry to process the data. (Mata Pavia et al., 2011a, 2011b, 2012).

819 *Co-registration with other modalities*

820 There are no fundamental limitations that prevent the possibility to
821 co-register fNIRS with other neuroimaging modalities. Multimodality
822 should be pursued aiming not only at validating fNIRS, but also at better
823 understanding the physiological processes following brain stimulation
824 (Yucel et al., 2012) and at the minimization of physiological noise
825 (Cooper et al., 2012b).

826 For instance TD fNIRS and electroencephalography (EEG) co-
827 registration has been performed both for validating the TD fNIRS
828 (Torricelli et al., 2011) and for the study of the neurovascular coupling
829 (Bari et al., 2012; Jelzow et al., 2010). Experiments have been performed
830 with pre-mounted EEG caps or mounting of individual electrodes. In
831 both cases no interferences have been reported, verifying that these
832 neuroimaging techniques can be easily applied and co-applied. More-
833 over results of the different techniques showed agreement between
834 them and with literature. In neurovascular coupling studies, fNIRS
835 allowed a reliable measure of oxy- and deoxyhemoglobin changes, per-
836 mitting the identification of a cascade of responses and the quantifica-
837 tion of temporal delays between electrical and vascular response. To
838 co-register TD fNIRS and functional magnetic resonance imaging
839 (fMRI), the TD fNIRS instrument should reside and be operated at a
840 safe distance from the fMRI scanner. Therefore, the use of long
841 (e.g. 10 m) optical fibers for light delivery and collection from the
842 head of the subject is required. As discussed, temporal dispersion
843 in the optical fibers introduces a degradation of the overall perfor-
844 mance of the TD fNIRS system. A reduction of the NA (e.g. by spatial
845 filtering the mode propagating in the outer part of the fiber bundle)
846 is useful to maintaining the IRF at acceptable FWHM values. This
847 comes unavoidably at the cost of a large loss of signal that has to
848 be compensated by the use of very sensitive detectors (Brühl et al.,
849 2005; Jelzow et al., 2009; Torricelli et al., 2007). Further, to fit the
850 limited space between the head and the MRI cage, 90° bended
851 optodes or prisms were used. The MR-compatible fNIRS systems
852 were successfully employed. The combination of the two modalities
853 introduced advantages for both sides: the analysis of optical data
854 was validated and improved by using MR results as prior knowl-
855 edge, while the calibration of the fMRI-BOLD signal could benefit
856 from the fNIRS measured parameters.

857 Similarly, in TD fNIRS and magneto-encephalography (MEG)
858 co-registration the use of 4.5 m long optical fiber bundles, mounted
859 tangentially to the subject's head via prisms, has been reported since
860 the instrument was positioned outside the magnetically shielded
861 room. A modulation-based DC-MEG technique was used with the bed
862 sinusoidally moved in a horizontal direction by a hydraulic piston.
863 Only minor movement amplitudes of the head of a few millimeters
864 were observed during the stimulation periods (Mackert et al., 2008;
865 Sander et al., 2007). In the reported papers, experiments were
866 performed in MEG/TD fNIRS coregistration to characterize the dynamics
867 of the interaction between the cortical neuronal and vascular responses.
868 The combined analysis provided not only a qualitative, but also a quan-
869 titative assessment of the temporal behaviors. Furthermore, the depth
870 resolution of TD fNIRS enabled the separation of systemic and cerebral
871 hemoglobin concentration changes. This eliminated the uncertainty of
872 previous MEG/CW fNIRS recordings, where signal contaminations by
873 extra-cerebral variations could not be excluded definitely.

874 Simultaneous co-registration of TD fNIRS and positron emission to-
875 mography (PET) were performed and no particular technical issues
876 were raised (Ohmae et al., 2006). A good correlation coefficient was
877 obtained between TD fNIRS-derived cerebral blood volume (CBV) and
878 PET-derived CBV, while the absolute CBV levels by TD fNIRS were
879 lower than those by PET.

880 TD fNIRS signals from cortical regions and changes in micro-
881 circulatory blood flow dynamics in the scalp as measured by laser
882 Doppler flowmetry (LDF) were simultaneously recorded in a couple of
883 recent studies (Aletti et al., 2012; Kirilina et al., 2012), strengthening

884 that the model-based separation of TD fNIRS early (superficial) and
885 late (deep) photons is able to cancel, or at least attenuate, the surface
886 confounding effects. Since LDF employs CW light sources, proper
887 solutions (e.g. use of filters, offset positioning of the probes,
888 time-multiplexing of the techniques) are required to avoid interference
889 on TD fNIRS signals. Same cautions should also be used when TD fNIRS is
890 simultaneously co-registered with another optical technique such as
891 diffuse correlation spectroscopy (Busch et al., 2012; Diop et al., 2011).

892 *Performance assessment and standardization*

893 The compelling need for standardization and quality assessment of
894 diffuse optics instruments is a key requirement for the translation of
895 new optical tools to effective clinical use (Hwang et al., 2012). The
896 definition of common procedures for the performance assessment of
897 instruments, implemented over a set of highly calibrated and reproduc-
898 ible phantoms is a key requirement for the grading of system perfor-
899 mances, the quantitative assessment of instrument upgrades, the
900 validation of clinical prototypes, the enforcement of quality control
901 and consistency in clinical studies, and the comparison of clinical results
902 performed with different instruments. Within the framework of different
903 European projects (MEDPHOT, OPTIMAMM, nEUROpt, LaserLabEurope),
904 common protocols and related phantom kits have been developed to
905 provide guidelines for the comparison of various diffuse optic systems.
906 In particular, the performance assessment of TD fNIRS instruments was
907 addressed in the nEUROpt project with the adoption of 3 protocols agreed
908 upon by a cluster of 17 institutions.

909 These include the “Basic instrumental performance” protocol to
910 characterize key hardware specifications of TD fNIRS systems (e.g.
911 FWHM of the IRF, drift of laser power or timing) that are crucial for
912 the outcome of the clinical measurements (Wabnitz et al., 2011).

913 The MEDPHOT protocol (Pifferi et al., 2005) was adapted to TD fNIRS
914 systems in order to characterize the capability of an instrument to mea-
915 sure the optical properties (absorption coefficient and reduced scattering
916 coefficient) of a homogeneous diffusive medium by assessing accuracy,
917 linearity, noise, stability, and reproducibility of these measurements.

918 Finally, the nEUROpt protocol was designed to address the capability
919 of optical brain imagers to detect, localize and quantify changes in the
920 optical properties of the brain (cerebral cortex) and to eliminate the in-
921 fluence of extra-cerebral tissues on the measurement. A specific inho-
922 mogeneous phantom was designed to reliably mimic absorption
923 changes in the cortex as the most relevant physical quantity in neuro-
924 logical applications of diffuse optical imaging (Wabnitz et al., 2013).

925 Common efforts are being currently pursued to further promote
926 standardization issues in the scientific community both for TD and
927 CW regimes. A joint initiative of the International Electrotechnical Com-
928 mission (IEC) and of the International Organization for Standardization
929 (ISO), led by Prof. Hideo Eda (The Graduate School for the creation of
930 new Photonics industries, Hamamatsu, Shizuoka, Japan), with the sup-
931 port of Physikalisch-Technische Bundesanstalt, Berlin and Politecnico di
932 Milano, Milan, for actions at the local (national) level in Germany and
933 Italy, has been started, aiming at defining a simple, easy to use standard.
934 The proposed project is carried out by technical committees ISO/TC 121/
935 SC 3 and IEC/SC 62D JWG 5 under the IEC lead (IEC, 2013).

936 Finally it is worth mentioning that TD fNIRS data type (as well as CW
937 and FD data types) will be inserted in the Shared Near Infrared File For-
938 mat Specification, a recent initiative for standardization of data types
939 triggered by the fNIRS community (Frederick and Boas, 2013).

940 **TD fNIRS features**

941 In this section we present the main features (or fingerprints) of TD
942 fNIRS, aiming at elucidating the differences and advantages with re-
943 spect to CW fNIRS and its drawbacks. We focus on the issues of quan-
944 tification, penetration depth, depth selectivity, spatial resolution, and
945 contrast-to-noise ratio. As a general aspect we note that these issues

are strongly entangled since the common underlying physical phenomenon is the interplay between light absorption and light diffusion at the microscopic scale. However, for the sake of clarity we try to distinguish the main peculiarity of each presented issue. We conclude this section with representative *in vivo* data obtained with a TD fNIRS system.

Quantification

Probably the oldest argument in favor of the TD approach is that of discrimination and quantification of the optical properties, namely the absorption coefficient and reduced scattering coefficient, the former being related to tissue constituents, the latter to tissue structures (Jacques, 1989b). Absolute estimate of the absorption coefficient would allow the derivation of SO_2 , a crucial parameter for many neurological conditions (Maas and Citerio, 2010).

However this advantage of TD NIRS strictly holds in a homogeneous medium. A TD NIRS measurement at a single source detector distance allows a complete optical characterization of the probed tissue, without the complicated multi-distance arrangements and the cumbersome calibration procedure that are needed for CW NIRS and FD NIRS. A few CW NIRS commercial systems have implemented a multi-distance approach (also called space-resolved spectroscopy, SRS) and yield parameters related to SO_2 , assuming a constant and spectrally flat scattering coefficient (Wolf et al., 2007).

When dealing with more complex geometries, the use of TD NIRS is likely to become less immediate. In a two-layered medium accurate estimate of the optical parameters have been obtained, provided a multi-distance (Martelli et al., 2003, 2004) or a multi-distance and multi-wavelength (Pifferi et al., 2001). TD approach is used. In the case of a real tissue, like the human head, a two-layered model could be a too simple approximation, and the use of priors of the true geometry (e.g. from anatomical 3D MRI maps or atlas), would be a prerequisite for setting up the forward problem by numerical methods like FEM or Monte Carlo. Absolute quantification of the optical properties in a real head is still an open issue. A recent collaboration among research groups in the framework of the European project nEUROpt is addressing the problem with a step by step approach involving multiple techniques (e.g. CW NIRS at multiple short distances to provide information on the superficial layer, to be used as priors for multi-distance and multi-wavelength TD NIRS in a layered model) (Foschum et al., 2012).

The two-layer approach was implemented on TD NIRS data on the adult head (Gagnon et al., 2008), and reported a clear distinction between extra- and intra-cerebral optical properties, even though the values could not be validated by independent modalities. In many applications of interest in the neuroimaging community fNIRS looks for changes with respect to a baseline. Only the few FD or SRS CW fNIRS systems, implementing the multi-distance approach, aim at providing absolute changes, while the majority of single source detector distance CW fNIRS devices just provide relative changes. TD fNIRS can be of help since, with limited assumptions on the baseline optical properties (a rough estimate can be always obtained by fitting with the homogeneous model), average photon path length (equivalently the average time spent by photon) can be estimated in different head compartments (at least the extra-cerebral and the intra-cerebral ones) allowing for absolute estimate of absorption changes. Expressions to estimate the absorption changes have been reported in Appendix A. In the following *Depth selectivity* section we will provide further comments on the quantification of absorption changes based on an experimental validation.

Penetration depth

For fNIRS applications aiming at mapping the functioning of human brain, the ability to probe the measured tissue in depth is of the utmost importance. NIRS light has in fact to cross through the scalp, the skull and the cerebrospinal fluid before reaching the

brain, and NIRS photons have to travel back to the head surface to be eventually detected. In the adult head the mean thickness of the skull has been measured in the range from 5.3 mm to 7.5 mm (Moreira-Gonzalez et al., 2006), and the average distance between the cortical surface and the head surface along the scalp was estimated to be in the range of 10–30 mm depending on the location (Okamoto et al., 2004).

To properly probe the cortical region a source–detector distance of 30–40 mm is typically used in many CW fNIRS devices, while shorter distances (20–30 mm) proved to be more efficient in newborns taken into account the reduced head size (Dehaes et al., 2011b; Gervain et al., 2011). This is in agreement with theoretical expectations. In CW NIRS, photons emerging at larger source detector distances have traveled longer paths deeper inside the medium, and thus they carry more information on deeper tissues (Del Bianco et al., 2002; Feng et al., 1995).

TD fNIRS measurements on adult have been typically reported with source–detector distance in the range of 20–30 mm. Indeed, in TD NIRS measurements the information on deeper tissues can be obtained from photons emerging with longer time-of-flight (Steinbrink et al., 2001), independently of the source detector distance (Del Bianco et al., 2002), as also demonstrated by the null distance TD NIRS approach (Pifferi et al., 2008; Spinelli et al., 2006; Torricelli et al., 2005).

Figs. 4 and 5 show the results of simulations performed to obtain the sensitivity profiles and maps for different source detector distances in a homogeneous medium and in a human head, respectively. It is evident that in both cases penetration depth increases with time and not with source detector distance.

Fig. 6 presents the results of a simple experiment (from the nEUROpt protocol) that can be effectively used to test penetration depth. A black PVC cylinder (volume 500 mm³) is embedded in a liquid diffusive medium with average optical properties mimicking a human head ($\mu_a = 0.01 \text{ mm}^{-1}$, $\mu_s' = 1.0 \text{ mm}^{-1}$). The cylinder is positioned in the mid plane between source and detector (at a distance of 30 mm) and its depth is varied in the range of 6–40 mm. The system setup is described in Contini et al. (2013a). As shown in Fig. 6(a), the contrast for an early time-gate (500 ps) is high if the perturbation is located close to the surface, while it diminishes rapidly as the perturbation depth increases. Conversely a late time-gate (e.g. 2500 ps) has a lower contrast for perturbation with shallow depth, while the contrast increases as a function of perturbation depth, reaching a maximum and then going to zero. We observe that the contrast is small but not negligible even at a depth of 30 mm for the late gate at 3500 ps. The contrast for the CW case (obtained by summing photons detected at any time) is also shown. The dependence of the contrast on the photon time-of-flight is plotted in Fig. 6(b) for different depths of the perturbation. It is clear that the optimum time-gate moves to longer time as the perturbation goes deeper in the medium, although the contrast inevitably diminishes.

Further, we recall that in CW fNIRS background absorption strongly affects penetration depth by preferentially reducing the number of long lived (i.e. deeper) photons. Instead, in TD fNIRS the penetration depth is independent from the background absorption (Del Bianco et al., 2002). Actually, a photon behaves in the same way independently from the used detection technique. Consequently, as shown in Fig. 1, in TD fNIRS an increase in absorption determines a reduction in the number of photons with longer time-of-flight (the longer the time-of-flight, the higher the probability of being absorbed). Hence absorption does have an effect on penetration depth in TD fNIRS since it reduces the temporal dynamics (at the microscopic level). Indeed this effect can be properly compensated by increasing the injected power (if available, and if within the safety limits). Nothing can be done in CW fNIRS to overcome the effect of background absorption. One could argue that it is unlikely that during an experiment the background absorption varies significantly. Unfortunately this could be the case for systemic (global) effects that affect blood perfusion. From a more technical point of

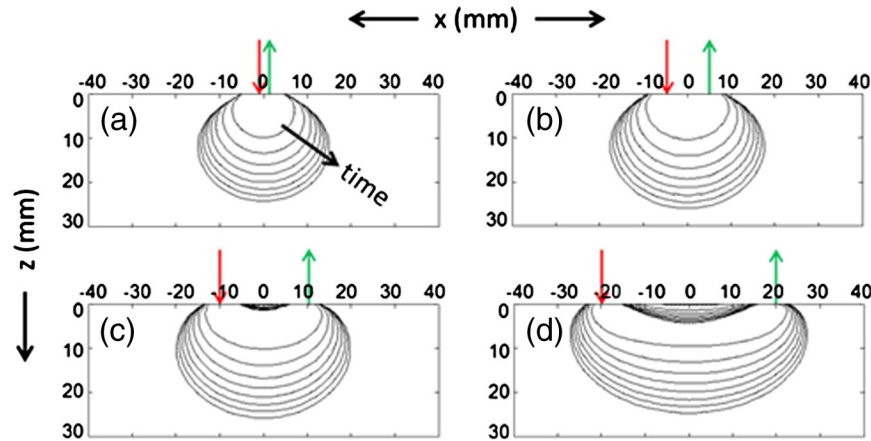


Fig. 4. Sensitivity profiles in a homogeneous medium. (a) Sensitivity profiles for TD reflectance in a homogeneous medium ($\mu_a = 0 \text{ mm}^{-1}$; and $\mu_s' = 1 \text{ mm}^{-1}$, $n = 1.4$) for different source detector distances ρ : (a) 2 mm; (b) 10 mm; (c) 20 mm; (d) 40 mm. Each line represents the contour edge of the contrast at 5% of the maximum, at a given time, from 500 to 4000 ps in steps of 500 ps. Source (red arrow) and detector (green arrow) positions are also shown. Simulations were performed with the analytical solution to the DE (Martelli et al., 2009).

1074 view, there is an advantage related to the independence of TD fNIRS
 1075 from background absorption. For a multi-wavelength approach, where
 1076 the use of spectral priors is aimed at improving the accuracy of the estimate
 1077 of hemodynamic parameters, the TD penetration depth will be to
 1078 a first approximation spectrally flat since it would depend only on the
 1079 smooth spectral dependence of the scattering.

1080 These considerations hold true not only in a homogeneous medium,
 1081 where the relationship among absorption, photon time-of-flight and
 1082 penetration depth can be obvious, but also in more complex situations

1083 such as a layered medium with different optical properties (e.g. the
 1084 human head).

1085 Depth selectivity

To improve depth selectivity, that is to reject superficial extra-
 1086 cerebral contributions, is a major challenge in fNIRS in both adults and
 1087 newborns (Aslin, 2013; Gagnon et al., 2012b; Kirilina et al., 2012;
 1088 Takahashi et al., 2011). In CW fNIRS this can be achieved by adding a
 1089 short distance (<5 mm) channel with enhanced sensitivity to superficial
 1090 layer (Gagnon et al., 2012a; Saager et al., 2011; Scarpa et al., in
 1091 press), or by means of a more sophisticated tomographic approach
 1092 exploiting a dense arrangement of the optodes (Eggebrecht et al.,
 1093 2012). Nonetheless, we stress that no depth selectivity is achievable
 1094 with a single source detector distance CW fNIRS device. Postural,
 1095 mechanical, and neural changes, which may occur under most investiga-
 1096 tive maneuvers, alter blood perfusion and/or distribution in the
 1097 extra-cranial compartment and affect CW fNIRS variables to the extent
 1098 that detected changes in cerebral tissue blood volume and oxygenation
 1099 can be frequently reversed (Canova et al., 2011).

1100 On the other hand, in single source detector distance (either large or
 1101 small) TD fNIRS depth selectivity is improved by contrasting the signal
 1102 obtained after integration of photons detected at early and late
 1103 time-windows (Contini et al., 2007; Selb et al., 2005), or, similarly, by
 1104 contrasting the moments of the DTOF (Hervé et al., 2012; Liebert et
 1105 al., 2004, 2012).

1106 A significant modification of the instrumentation is required in CW
 1107 fNIRS to implement the multi-distance approach. Conversely, since TD
 1108 fNIRS naturally measures photon time-of-flight, it just requires post
 1109 processing analysis to discriminate intra-cranial and extra-cranial
 1110 contributions. The TD approach based on time-windows or moments is
 1111 also efficient for identifying other artifacts related to superficial phe-
 1112 nomena, e.g. the detachment of an optode (Gibson et al., 2006).

1113 A simple experiment (from the nEUROPT protocol) can be devised to
 1114 test depth selectivity. In a two-layer diffusive phantom (see Del Bianco
 1115 et al., 2004 for details on the construction of the phantom) absorption
 1116 changes either in the upper or in the lower layer have been produced
 1117 by adding known amounts of a calibrated black ink. The corresponding
 1118 contrasts for different time-gates (constant width: 500 ps, increasing
 1119 delay: 500, 1000, 2000, and 4000 ps) and for the CW case (delay: 0 ps,
 1120 width: 0–5000 ps), have been calculated according to Formula A1
 1121 reported in Appendix A and are shown in Fig. 7. When the absorption
 1122 changes in the upper layer, all time-gates are affected (all photons
 1123 travel in the superficial layer since they are injected from the external
 1124

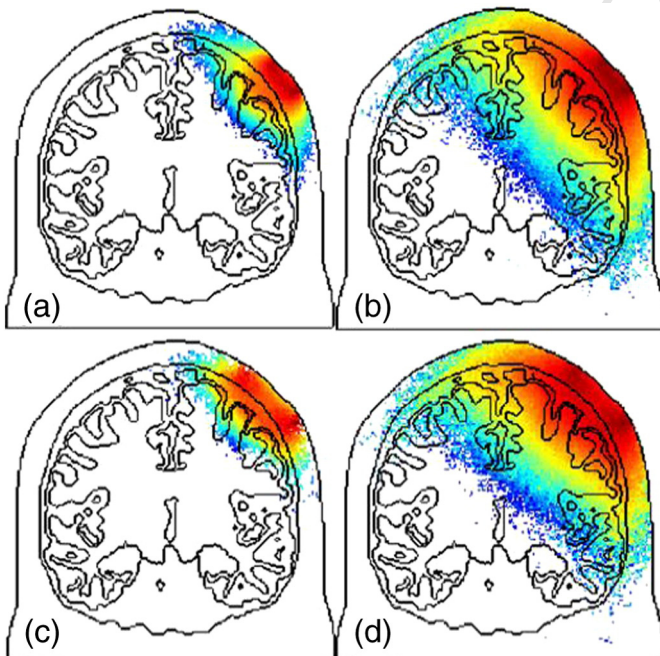


Fig. 5. Sensitivity maps in a head model for different source detector distances and time-gates. (a) $\rho \approx 20 \text{ mm}$, $t = 1000 \text{ ps}$; (b) $\rho \approx 20 \text{ mm}$, $t = 5000 \text{ ps}$; (c) $\rho \approx 40 \text{ mm}$, $t = 1000 \text{ ps}$; (d) $\rho \approx 40 \text{ mm}$, $t = 5000 \text{ ps}$. Monte-Carlo forward simulations in a segmented volumetric 3D domain based on a digital head (Collins et al., 1998) have been calculated using 10^6 launched photons. We chose realistic optical properties for the brain structures (Boas et al., 2005). The photons have been simulated as leaving light sources positioned over C1, C3h and C3 positions of the 10/20 system. Sensitivity maps were then calculated via time convolution of forward solutions for pairs C3–C3h ($\rho \approx 20 \text{ mm}$) and C3–C1 ($\rho \approx 40 \text{ mm}$).

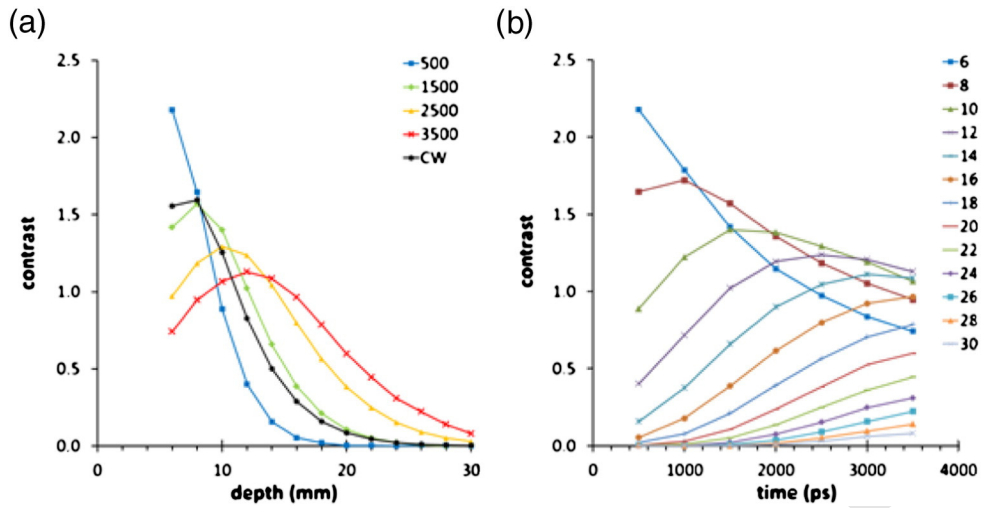


Fig. 6. Penetration depth. (a) Contrast as a function of depth of the perturbation for different time-gates (constant width: 500 ps, increasing delay: 500, 1500, 2500, and 3500 ps), and for the CW case (delay: 0 ps, width: 0–4500 ps); (b) Contrast as a function of time (at the DTOF scale) for different depths of the perturbation. Background medium: $\mu_a = 0.01 \text{ mm}^{-1}$, $\mu_s' = 1.0 \text{ mm}^{-1}$; $\rho = 30 \text{ mm}$; perturbation: black PVC cylinder (volume = 500 mm^3) positioned at different depths in the mid plane between source and detector. Formula A1 was used for calculating the contrast.

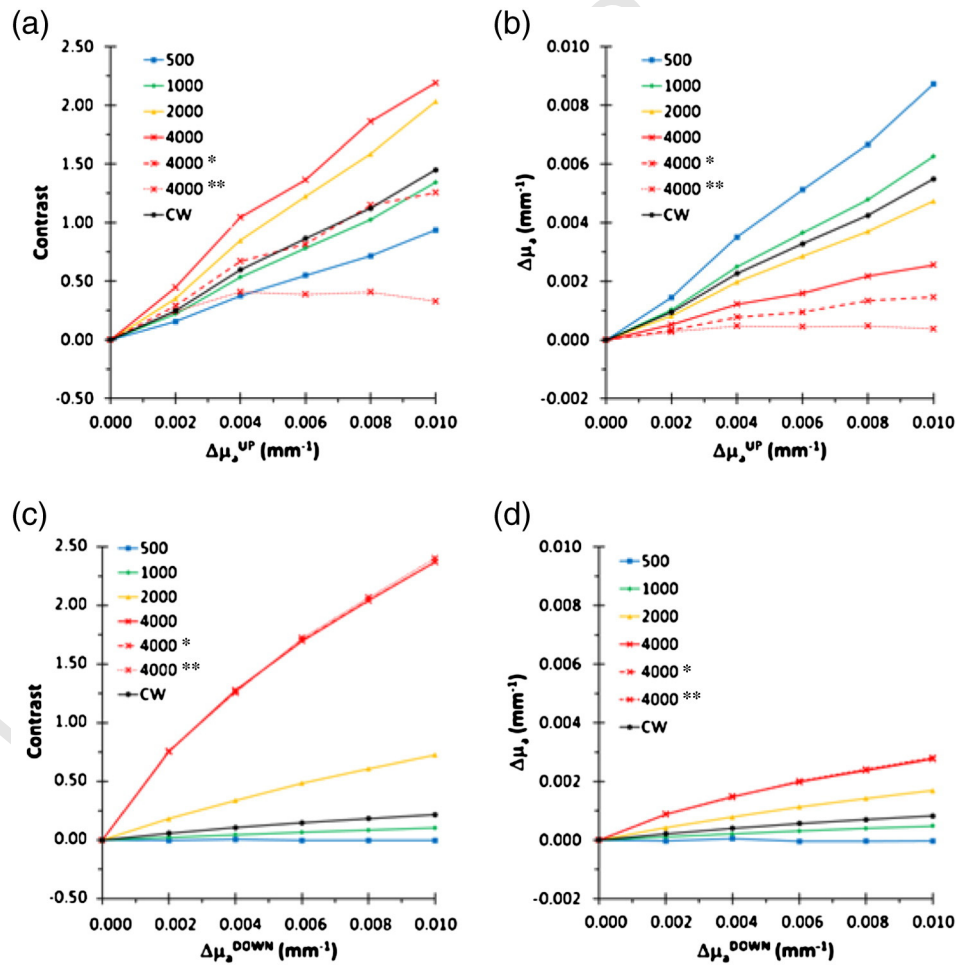


Fig. 7. Depth selectivity. Contrast (left column) and estimated absorption changes (right column) in a two layered medium (upper layer thickness = 10 mm, lower layer thickness = 40 mm) for different time-gates (constant width: 500 ps, increasing delay: 500, 1000, 2000, and 4000 ps), and for the CW case (delay: 0 ps, width: 0–5000 ps). Top row: absorption was changed only in the upper layer. Bottom row: absorption was changed only in the bottom layer. For both cases, but only for the latest time-gate (delay: 4000 ps, width: 500 ps) we have also applied the corrections A6 and A7 introduced by Selb et al. (2005) and Contini et al. (2007), indicated with "*" and "**", respectively. Background medium: $\mu_a = 0.01 \text{ mm}^{-1}$, $\mu_s' = 1.0 \text{ mm}^{-1}$; $\rho = 30 \text{ mm}$.

upper surface). In particular we observe that the contrast is even higher for late gates, since long lived photons have a higher probability of being absorbed, independently of the location of the absorption perturbation. When the absorption changes are produced in the lower layer, the early gates have negligible or small contrast, as expected, since they have a reduced probability to reach the lower layer and then be reemitted at the surface. The contrast for the CW case is also reported and it is in general closer to the early than to the late gates (the majority of photons are in fact collected at early gates and they contribute largely to the CW signal). The changes in the absorption coefficient are then estimated with the Formulas A3–A7 reported in Appendix A. The use of an early time-window can provide a sufficiently accurate estimate of the absorption changes when they affect the upper layer (see Fig. 7(b)). In the same situation, a very late time-window is able to yield an estimate of the absorption changes in the lower layer that is minimally affected by the changes in the upper layer (especially if correction methods, described by Eqs. (A6) and (A7) are used). The problem of accuracy related to the estimate of photon path-length in the different layers of the medium is still an open issue in the case of changes affecting the lower layer. As shown in Fig. 7(d), linearity with the perturbation is achieved, but quantification is definitely poor. Nonetheless, the estimates obtained with the TD approach are catching the phenomenological effects occurring either in the upper or in the lower layer. More accurate estimates could be obtained with methods based on the moments of the DTOF (Liebert et al., 2012).

1150 Spatial resolution

1151 Light diffusion is the enabling mechanism in fNIRS since it allows
1152 photons to penetrate deeply in biological tissues and to be diffusely
1153 reemitted, carrying the information on deep structures. However,
1154 light diffusion itself strongly limits the achievable spatial resolution
1155 in fNIRS to a value of the order of 10 mm (Boas et al., 1994).

1156 When dealing with spatial resolution in fNIRS it is useful to distin-
1157 guish between lateral and depth resolution. Lateral resolution de-
1158 pends on source detector distance, therefore it can be improved by
1159 the use of multi-distance or tomographic detection schemes in both
1160 TD and CW fNIRS (Arridge et al., 2011; Gao et al., 2004) or of the
1161 null distance approach in TD fNIRS (Torricelli et al., 2005). This pa-
1162 rameter is also influenced by penetration depth and depth selectivity,
1163 therefore comparisons of lateral resolutions should be made at a fixed
1164 depth, typically 10 mm to mimic the average equivalent distance of
1165 brain cortex to the scalp (Wabnitz et al., 2013).

1166 Depth resolution explores the direction orthogonal to and beneath
1167 the (head) surface. In TD fNIRS depth resolution depends on photon
1168 time-of-flight and scattering properties (Liebert et al., 2004; Spinelli
1169 et al., 2009b; Steinbrink et al., 2001), while for CW fNIRS it depends on
1170 source detector distance, scattering and absorption (Del Bianco et al.,
1171 2002). Similarly to lateral resolution, depth resolution can be influenced
1172 by the ability of the system to reject confounding superficial phenome-
1173 na (i.e. extra-cerebral, systemic responses).

1174 Broadening of the IRF has detrimental effects on depth resolution as
1175 well as on penetration depth, depth selectivity, and contrast, and its in-
1176 fluence is larger for smaller source detector distance (Pifferi et al.,
1177 2010). A simple intuitive reason for this later aspect is the fact that
1178 the larger the source detector distance, the broader in time the mea-
1179 sured DTOF is compared to the IRF.

1180 If a better system with a narrower IRF cannot be designed, the possi-
1181 bility remains to partially overcome these limitations by employing con-
1182 volution or deconvolution procedures. Convolution of the IRF with a
1183 theoretical model before fitting experimental DTOF proved to be effec-
1184 tive for an accurate estimate of optical properties (Cubeddu et al.,
1185 1996; Spinelli et al., 2009a). In the past, deconvolution algorithms had
1186 the reputation of introducing noise in the computation and were rarely
1187 used. Recently improved deconvolution algorithms have been developed
1188 and tested (Bodi and Bérubé-Lauzière, 2009; Diop and St Lawrence,

2012; Hebden et al., 2003). To tackle the IRF problem, an elegant
method is the use of moments of the DTOF since no deconvolution
of the DTOF by the measured IRF is needed. The moments calculated
from the measured DTOFs can, in fact, be corrected for the IRF simply
by subtracting the corresponding moments of the IRF to obtain the
true moments (Hervé et al., 2012; Liebert et al., 2004). However,
since the moments are global parameters calculated by integrating
the DTOF (therefore mixing early and late arriving photons), this
semi-empirical approach can not totally circumvent the uncertainty
in photon timing due to a broad IRF, therefore depth resolution is not
likely to improve.

1200 Finally, we observe that for TD fNIRS the fundamental physical
1201 limit to depth resolution is imposed by scattering. In the ideal case
1202 of a delta-like IRF (in practice a temporal resolution of <1 ps that
1203 could be obtained, for instance by using ultrafast laser with fs pulse
1204 duration and a streak camera system, coupled to zero dispersion opti-
1205 cal fibers), it would be impossible to discriminate deep absorbing
1206 structures with a resolution better than 5 mm. The possibility to finely
1207 discriminate deep structures in diffusive media is therefore limited
1208 to the very superficial layers (i.e. depth \ll 5 mm), but in this case
1209 other advanced optical techniques like optical coherence tomography
1210 (Aguirre et al., 2006; Fujimoto et al., 1995) and laminar optical to-
1211 mography (Dunn and Boas, 2000; Hillman et al., 2004) are able to
1212 provide sharp results. These methods can be used for in vivo optical
1213 imaging of the exposed cortex. A review on the effect of light scatter-
1214 ing on depth resolution is provided by Hillman et al. (2011).

1215 Contrast-to-noise ratio

1216 The overall ability of an fNIRS system of detecting a cortical response
1217 depends on many factors (e.g. depth, simultaneous presence of superfi-
1218 cial systemic response, IRF), as discussed in the previous sections. A sin-
1219 gle parameter to synthetically gage an fNIRS system can be the
1220 contrast-to-noise ratio (CNR). The CNR takes into account the sensitiv-
1221 ity of the system to changes in the measured quantity (e.g. light atten-
1222 uation in CW fNIRS, intensity integrated in a given time-window in TD
1223 fNIRS) and it relates this change (contrast) to the noise level, as deter-
1224 mined – for instance – by the standard deviation of the measured quan-
1225 tity, typically estimated during a resting period (baseline).

1226 The contrast for a TD fNIRS measurement can be higher than for
1227 the CW case, simply because it is possible to extract long-lived pho-
1228 tons that have traveled a larger fraction of their path in the deeper
1229 cortical region as compared to the mean photon distribution collected
1230 in a CW measurement. Also, tighter spatial confinement attainable
1231 upon reducing the source detector distance – for a fixed photon trav-
1232 eling time – leads to an increase in contrast.

1233 Conversely, the real bottleneck of actual TD systems is the
1234 noise level. If the TCSPC technique is used – possibly the most popular
1235 choice – the maximum count rate per channel is limited to a few
1236 10^6 photons/s due to the single-photon counting statistics and mini-
1237 mum dead time of the electronics. This limits the maximum signal
1238 level that can be extracted in a TD measurement and thus constrains
1239 the CNR. Further, amplitude stability and overall detection responsivity
1240 are typically worse in a TD system simply because the need to achieve
1241 temporal information reduces the choice of sources and detectors. Fi-
1242 nally, the total number of parallel running sources and detectors is typi-
1243 cally lower due to the intrinsic higher complexity and cost of single
1244 devices.

1245 Fig. 8 shows the CNR as a function of depth for different time
1246 gates. We observe that the CNR value reported for the CW case is
1247 not the best estimate, since CW data have been obtained with a TD
1248 system by integrating all the detected photons. We expect that a
1249 real CW system performs in a much better way. An experimental
1250 comparison of the TD and CW approaches would be appropriate,
1251 but it is not within the scope of this review.

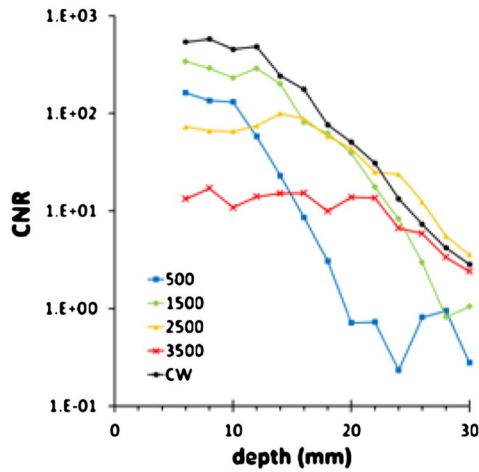


Fig. 8. Contrast-to-noise ratio. Contrast-to-noise ratio (CNR) as a function of depth, for different time gates (constant width: 500 ps, increasing delay: 500, 1500, 2500, and 3500 ps), and for the CW case (delay: 0 ps, width: 0–4500 ps); Background medium: $\mu_a = 0.01 \text{ mm}^{-1}$, $\mu_s' = 1.0 \text{ mm}^{-1}$; $\rho = 30 \text{ mm}$; perturbation: black PVC cylinder (volume = 500 mm^3) positioned at different depths in the mid plane between source and detector. Formula A1 was used for the calculation of the contrast.

For both studies the TD fNIRS medical device (working at 690 nm and 830 nm) described in Contini et al. (2006) was used, a single channel (source detector distance 20 mm) was centered over the C3 point, and data were acquired at 1 Hz.

In the motor task experiment the protocol consisted a 20 s baseline, 20 s finger tapping with the right hand at 2 Hz, and 40 s recovery. Ten repetitions were performed and averaged. In the Valsalva maneuver experiment the protocol consisted a 20 s baseline, 20 s expiring through a closed mouthpiece, and 40 s recovery. Five repetitions were performed and averaged.

In both experiments, for each wavelength and all repetitions, we calculated the contrast C, the absorption changes in the intra-cerebral and extra-cerebral region, and the O₂Hb and HHb time courses as described in Appendix A.

Figs. 9(a–g) report the contrast C during the finger tapping experiment for different time-gates with constant width (250 ps) and increasing delay (from 0 to 1000 in 250 ps steps, then 1500 ps and 2000 ps). For both 690 nm and 830 nm the contrast is rather flat and close to zero during the baseline, as expected. Then during the task it increases at 830 nm, while it decreases at 690 nm. These changes are greater for later time-gates. The maximum value of the contrast during the task period at 830 nm in fact almost doubles its value, from 0.04 at the earliest gate (delay 0 ps) to 0.07 for the latest time-gate (delay 2000 ps). Similarly, at 690 nm the contrast is three times higher at the latest time-gate ($C = -0.06$) with respect to the earliest time-gate ($C = -0.02$). This is an indication that a deep perturbation is present. Indeed by looking at the contrast at the very early time-gates, it is possible to observe that the contrast at 830 nm presents large periodic changes, only partially related to the

1252 *Representative in vivo data*

1253 To better illustrate the specific information that can be obtained
1254 by TD fNIRS we report on two simple case studies: a motor task exper-
1255 iment and a Valsalva maneuver.

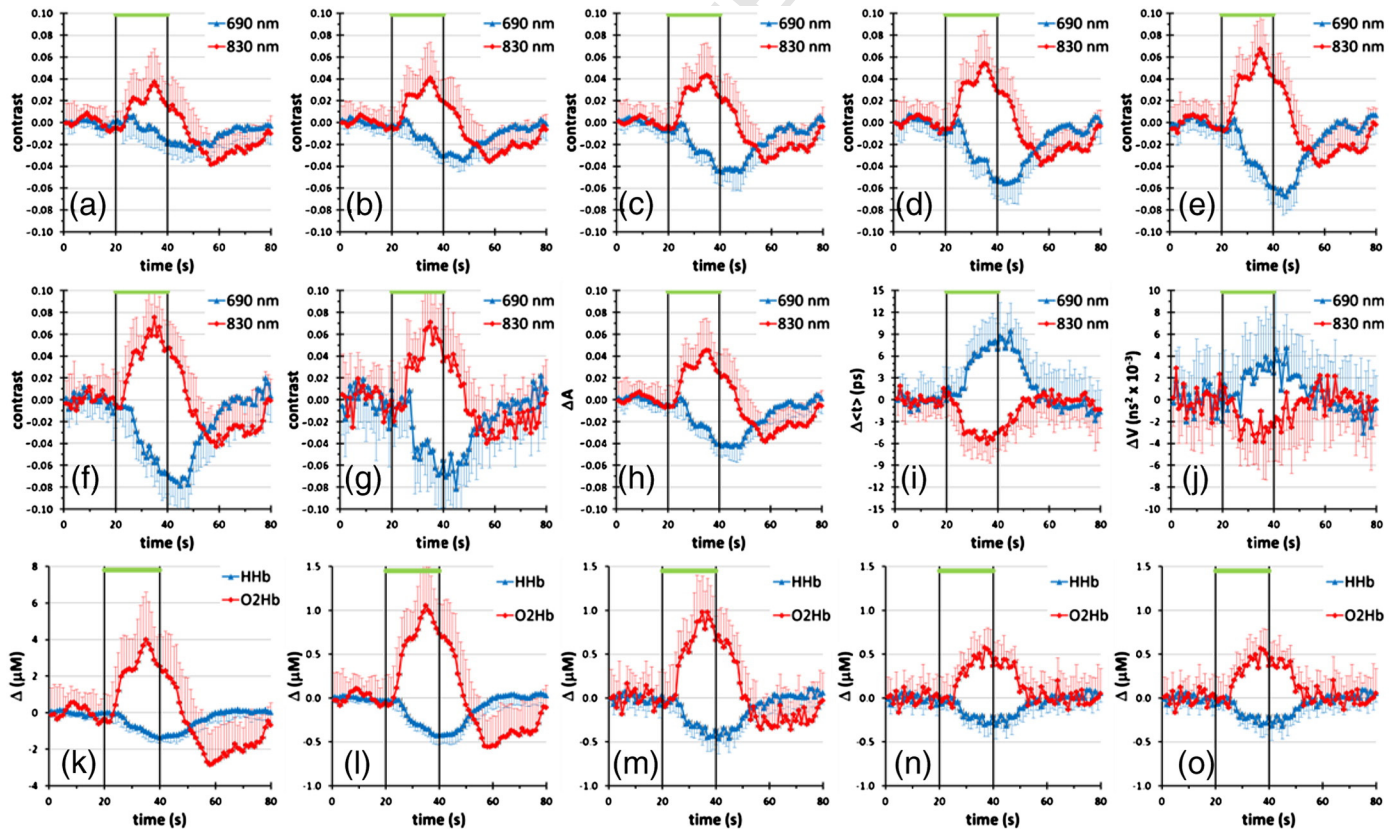


Fig. 9. Finger tapping experiment. Contrast at 690 nm (blue) and 830 nm (red) for different time-gates with constant width (250 ps) and increasing delay: (a) 0 ps, (b) 250 ps, (c) 500 ps, (d) 750 ps, (e) 1000 ps, (f) 1500 ps, (g) 2000 ps. Contrast for the moments of the DTOF: (h) 0th order moment, (i) 1st order moment, (j) 2nd order moment. Estimated changes in HHb (blue) and O₂Hb (red) as calculated from photons integrated in: (k) an early time window (delay: 0 ps, width: 500 ps, mean time-of-flight: 250 ps); (l) for the CW case (delay: 0 ps, width: 2500 ps); (m) a late time window (delay: 1750 ps, width: 750 ps, mean time-of-flight: 2125 ps); (n) late time window (delay: 1750 ps, width: 750 ps) with correction for changes in early time window (delay: 0 ps, width: 500 ps), Formula A6; (o) same as (n), but Formula A7. Average and standard deviation over 10 repetitions are shown for all plotted parameters. The black vertical lines and the green horizontal line mark the task period.

1285 task, with a triangular or saw-tooth shape, not resembling a typical
 1286 task-evoked cerebral hemodynamic response. We note that the
 1287 same time course is present at least qualitatively also at longer
 1288 time-gates, and this is expected since superficial changes affect
 1289 photons detected at any time, as described in previous sections. Con-
 1290 versely, the time course for 690 nm does not present this features. As
 1291 recently reported by Kirilina et al. (2012), this could likely be the ef-
 1292 fect of task-evoked systemic changes.

1293 Figs. 9(h–j) report the time course of the moments of the DTOF.
 1294 The contrast from the lowest order moment (related to the CW intensi-
 1295 ty) is greatly affected by systemic changes, while higher order mo-
 1296 ments are less affected.

1297 Figs. 9(k–o) report the time course for the estimates of O₂Hb and
 1298 HHb for the extra-cerebral region, for the intra-cerebral region (without
 1299 and with correction for changes in the extra-cerebral region), and the
 1300 global estimate from the CW case. In the extra-cerebral region the
 1301 O₂Hb signal presents the task-evoked changes, while the HHb presents
 1302 a limited decrease. In the intra-cerebral region the task-evoked pertur-
 1303 bation in O₂Hb still appears, while it is almost canceled if we use the
 1304 correction for the superficial disturbances. In the CW, the systemic
 1305 task-evoked effect is clearly visible.

1306 Figs. 10(a–g) report the contrast C during the Valsalva maneuver for
 1307 different time-gates with constant width (250 ps) and increasing delay
 1308 (from 0 to 1000 in 250 ps steps, then 1500 ps and 2000 ps). For both
 1309 690 nm and 830 nm the contrast during the task greatly increases
 1310 with respect to the baseline period. This holds true at any time-gate,
 1311 with a limited increase when moving from early to late gate: the con-
 1312 trast at 690 nm changes from 0.15 to 0.25, at 830 nm from 0.10 to

0.15. This suggests the presence of a superficial absorption perturbation
 with a limited effect on deeper regions, as expected (Canova et al.,
 2011). This is confirmed by the time courses of the moments of the
 DTOF (see Figs. 10(h–j)) and by the time courses of O₂Hb and HHb for
 the extra-cerebral region and for the intra-cerebral region, if for the lat-
 ter case the correction for changes in superficial layers is applied. We
 note that both the uncorrected intra-cerebral response and the CW re-
 sponse are largely affected by the superficial effects (see Figs. 10(k–o)).

Future perspectives

In this section we briefly present the foreseen advances at both the
 technological and modeling levels from which TD fNIRS could benefit in
 the next years.

There are several technological improvements in light sources, de-
 tection techniques and delivery and collection systems that could sig-
 nificantly enhance TD fNIRS's overall performances in the next years.

The SC fiber laser (Fianium UK Ltd., 2013b; NKT Photonics, 2013b)
 has been recently introduced in TD fNIRS systems and their potential
 has not been fully proved. They are compact and could nicely fit in a
 trolley and a rack for medical device. They provide narrow pulses at
 any level of power, without degrading the IRF. Indeed, they are to
 some extent a very inefficient solution since the available power is
 spread over a wavelength range much larger than the useful range.
 On the one hand, excess power in unused wavelength intervals (e.g.
 <600 nm, >900 nm) has to be properly attenuated (e.g. by using di-
 chroic mirror or hot filter) so as not to direct it to the sample under
 test. On the other hand, power spectral density is limited and

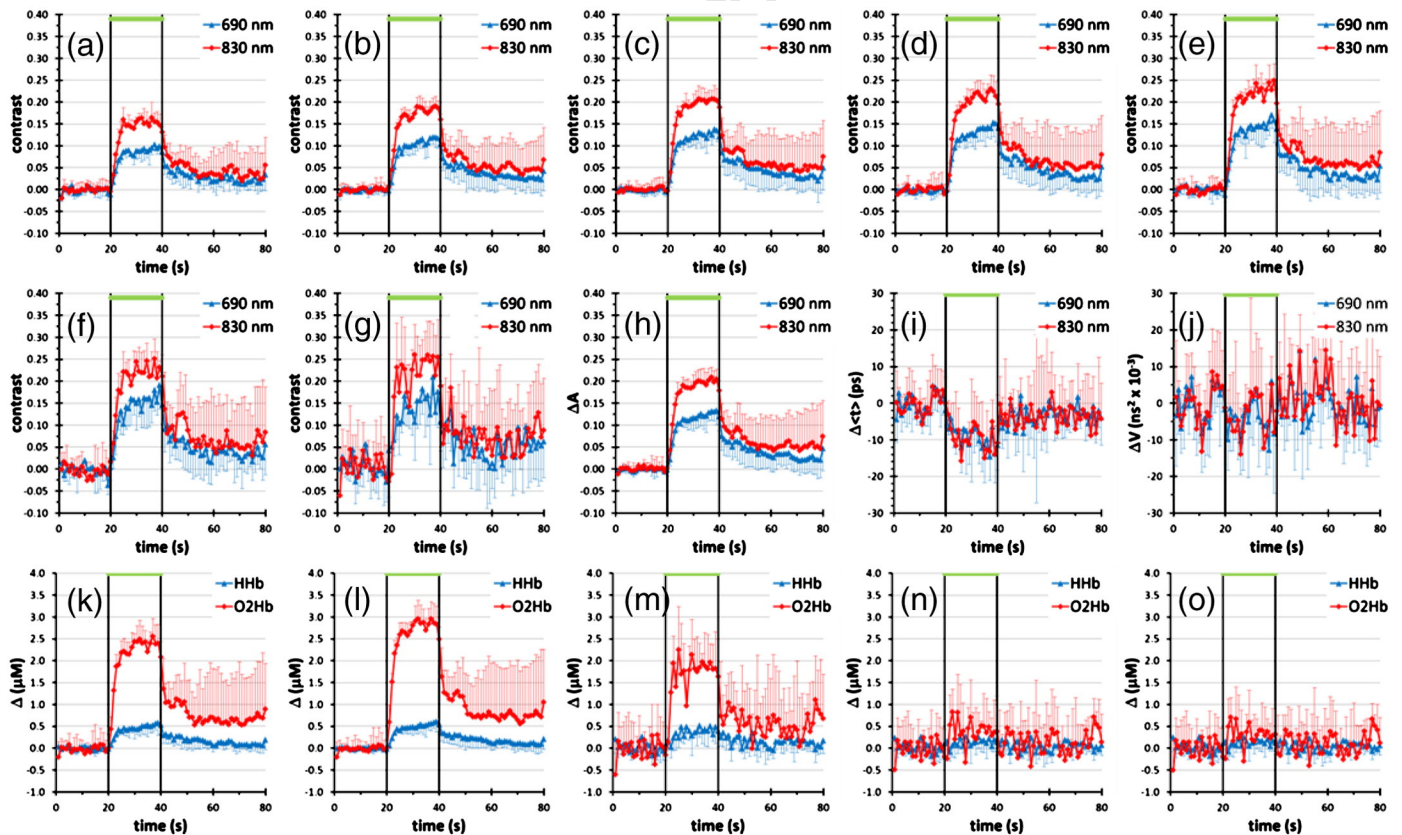


Fig. 10. Valsalva maneuver experiment. Contrast at 690 nm (blue) and 830 nm (red) for different time-gates with constant width (250 ps) and increasing delay: (a) 0 ps, (b) 250 ps, (c) 500 ps, (d) 750 ps, (e) 1000 ps, (f) 1500 ps, (g) 2000 ps. Contrast for the moments of the DTOF: (h) 0th order moment, (i) 1st order moment, (j) 2nd order moment. Estimated changes in HHb (blue) and O₂Hb (red) as calculated from photons integrated in: (k) an early time window (delay: 0 ps, width: 500 ps, mean time-of-flight: 250 ps); (l) for the CW case (delay: 0 ps, width: 2500 ps); (m) a late time window (delay: 1750 ps, width: 750 ps, mean time-of-flight: 2125 ps); (n) late time window (delay: 1750 ps, width: 750 ps) with correction for changes in early time window (delay: 0 ps, width: 500 ps), Formula A6; (o) same as (n), but Formula A7. Average and standard deviation over 5 repetitions are shown for all plotted parameters. The black vertical lines and the green horizontal line mark the task period.

sufficient power levels for application in the real environment are obtained summing up the power at adjacent wavelengths (up to 40 nm in some cases), at the cost of reducing the spectral purity of the injected pulses, and the overall accuracy in the reconstruction if the bandwidth is not taken into account (Farina et al., 2009). Consequently, a SC with reduced width, covering the proper spectral range while maintaining a high conversion rate, is desirable.

As an alternative to SC lasers, picosecond pulsed laser diode heads based on a master oscillator fiber amplifier concept can offer pulse widths <100 ps and average powers up to 1 W (depending on wavelength). The drawback at the moment of writing is the limited availability of wavelengths (e.g. 531 nm, 710 nm, 766 nm, 1064 nm and 1530 nm) (Fianium UK Ltd., 2013a; PicoQuant GmbH, 2013c).

The silicon photonics field is promising compact and scalable devices and components for telecommunications, but unfortunately they are not produced in the wavelength range of interest for fNIRS (Fang and Zhao, 2012). Similarly several optical components and devices for properly handling light pulses at the picosecond level have been devised in the fields of photonics and communications by exploiting the recent studies on metamaterials (Liu and Zhang, 2011), and chalcogenide materials (Eggleton et al., 2011). Again, there are no fundamental limitations that prevent the designing of specific components for operation in the spectral range of interest for fNIRS.

Also delivery and collection systems could be positively influenced by the advances in Photonics. To mention a specific case, we observe that nowadays commercial products exist that are able to overcome some of the basic limitations of classical optical fiber. Photonic crystal fibers (PCF) have in fact been recently produced operating as single mode over a broad spectral range (NKT Photonics, 2013a). A conventional single mode optical fiber is actually multimode for wavelengths shorter than the second-mode cutoff wavelength, limiting the useful operating wavelength range in many applications. With PCF we could think to overcome most of the limitations of multimode SI fiber bundles that are used for light collection in TD fNIRS.

For what concerns the detection techniques, we observe that the main drawbacks of existing TCSPC systems are actually not set by physical limits, and they could be overcome by technological advancements. As a side product of the research on the null distance TD approach, ultra-fast time gating circuits and electronics have been developed, that could improve the performances of modern detection techniques like TCSPC (the limits in photon counting statistics holds but with the time gating approach we are for example able to count only useful photons in specific time-windows). In particular time-to-digital conversion (TDC) electronics, could replace modern TCSPC modules for aiming at a higher integration level (Mata Pavia et al., 2012). Similarly advanced photodetectors, like SPAD with enhanced sensitivity, large area SPAD, SPAD array or matrix with improved performances could be designed and fabricated (Micro Photon Devices, 2013a, 2013c).

Similarly, the modeling used for the interpretation of real data is nowadays too elementary. Advanced computational tools for modeling light propagation in the head are available, but to date they have been used mostly for simulations, while rarely for the in vivo data analysis. The situation is different for the CW case where sophisticated approaches to data analysis have been successfully proposed (Cooper et al., 2012a; Custo et al., 2010; Tsuzuki et al., 2007, 2012). In most clinical studies the head is approximated as homogeneous or two layered medium. This approach might have the advantage of robustness but it definitely fails in terms of accuracy. The use of priors (e.g. anatomical, optical, or spectral) would greatly improve the accuracy of the results, but in most cases at the cost of a very high computational load. Parallel computing algorithms and platforms are therefore required to make this affordable.

Conclusions

We have presented a comprehensive and critical review on TD fNIRS in which we have highlighted that TD fNIRS could play a

significant role not only as a complex research tool at the laboratory stage, but also as a powerful instrument for all fNIRS applications.

As a general comment we note that an ideal TD fNIRS system might not exist. However, the design of novel instruments can be properly tailored to the specific needs of the end-users at both research and clinical levels. The performances, the complexity, as well as the costs of a TD fNIRS system can significantly vary depending for example on the number of independent channels.

Interestingly, TD NIRS systems and devices have found applications in other fields such as optical mammography, and molecular imaging of small animals. The eventual growth and broader diffusion of these applications would further foster TD fNIRS. By synergic and collaborative efforts among experts in Photonics, Electronics, Information technology and Neuroscience we foresee a flourishing future for TD fNIRS.

We persuasively conclude this review by quoting the 17th century English philosopher and scientist Francis Bacon: "Truth is rightly named the daughter of *time*" (Novum Organum, 1620).

Uncited references

- Boas and Dale, 2005 1421
 Hielscher et al., 2000 1422
 Micro Photon Devices, 2013b 1423

Acknowledgments

The Authors are thankful to many colleagues and friends for helpful and illuminating discussions during the past years. We would like to kindly mention: Prof. Rinaldo Cubeddu, Alberto Dalla Mora, Laura di Sieno (Politecnico di Milano, Dipartimento di Fisica); Fabrizio Martelli and Giovanni Zaccanti (University of Florence, Italy); Alberto Tosi and Franco Zappa (Politecnico di Milano, Dipartimento di Elettronica ed Informazione). In addition all researchers in the narrow TD fNIRS community, with special remarks for Heidrun Wabnitz and Rainer Macdonald (Physikalisch-Technische Bundesanstalt, Berlin, Germany), Adam Liebert and Roman Maniewski (Institute of Biocybernetics and Biomedical Engineering, Warsaw, Poland), Alwin Kienle (Institut für Lasertechnologien in der Medizin und Meßtechnik an der Universität Ulm, Germany), Hellmuth Obrig (Max-Planck-Institut für Kognitions- und Neurowissenschaften, Leipzig, Germany), Jens Steinbrink (Charité Universitätsmedizin, Berlin, Germany), Jeremy Hebden and Simon Arridge (University College London, United Kingdom), Juliette Selb and David Boas (Massachusetts General Hospital, Athinoula A. Martinos Center, Charlestown, Massachusetts). A particular thanks also to Martin Wolf (University Hospital Zurich, Switzerland), Jacques Mehler (Scuola Internazionale Superiore di Studi Avanzati, Trieste, Italy), Luciano Fadiga (University of Ferrara, Italy), Patrizia Baraldi (University of Modena, Italy) and Simone Cutini (Università di Padova). Finally, Marco Ferrari and Valentina Quaresima (Università di L'Aquila, Italy) have supported with their passion and expertise our steps in the fNIRS field.

The research leading to these results has partially received funding from the European Community's Seventh Framework Programme under the nEUROpt Project (grant agreement FP7-HEALTH-2007-201076).

Conflict of interest

The Authors have no relationships with the commercial companies cited in the paper that could inappropriately influence, or be perceived to influence, their work.

Appendix A

The concentration changes of O₂Hb and HHb were obtained from the changes in light attenuation after integrating photons in different time-windows.

1463 For each wavelength, we calculated the contrast, defined as

$$C(d, w; T; \lambda) = -\ln[N(d, w; T; \lambda)/N_0(d, w; \lambda)] \quad (A1)$$

1463 where $N(d, w; T; \lambda)$ is the number of photons collected in a time window
1466 with delay d and width w , at macroscopic (experiment) time T for
1467 wavelength λ , and $N_0(d, w; \lambda)$ is the number of photons collected in
1468 the very same time window and for the same wavelength, averaged
1469 over the baseline period of the protocol.

1470 Changes in the absorption coefficient for each wavelength λ and at
1471 any time T are estimated with the formula

$$\Delta\mu_a(T; \lambda) = C(d, w, T; \lambda)/L \quad (A2)$$

1473 where L is the photon path-length (Nomura et al., 1997).

1474 A rough assumption for the path-length is $L = vt$, where v is the
1475 speed of light in the medium and t is the average photon-time-
1476 of-flight. Taking into account the dependence of penetration depth on
1477 photon time-of-flight, by properly selecting an early time-gate it is possible
1478 to estimate changes in more superficial layers (i.e. extra-cerebral),
1479 while a late time-gate yields information on deeper regions (i.e.
1480 intra-cerebral). The formulas for the absorption changes can then be
1481 specified as follows:

$$\Delta\mu_a^{\text{EXTRA}}(T; \lambda) = C(d_E, w_E; T; \lambda)/L_E \quad (A3)$$

$$\Delta\mu_a^{\text{INTRA}}(T; \lambda) = C(d_L, w_L; T; \lambda)/L_L \quad (A4)$$

1483 where d_E , w_E , and L_E (d_L , w_L , and L_L) are proper delay, width and
1486 path-length of the time-gate to select early (late) arriving photons.

1487 By integrating all detected photons (e.g. selecting a time-window
1488 with delay $d_{CW} = 0$ ps and width $w_{CW} = 5000$ ps) it is possible to
1489 address the CW case. As photon path-length we use $L_{CW} = v \langle t \rangle$,
1490 where $\langle t \rangle$ is the mean time-of-flight (first order moment of the
1491 DTOF). The corresponding absorption change is then calculated as

$$\Delta\mu_a^{\text{CW}}(T; \lambda) = C(d_{CW}, w_{CW}; T; \lambda)/L_{CW} \quad (A5)$$

1493 This is equivalent to the modified Beer–Lambert law with differential
1494 path-length factors (DPF) not taken from the literature but estimated
1495 directly by the DTOF.

1497 To enhance the contribution from deep layers and to remove possible
1498 disturbances caused by superficial ones, correction methods (Contini et
1499 al., 2007; Selb et al., 2005) are also used for the intra-cerebral changes:

$$\Delta\mu_a^{\text{INTRA}}(T; \lambda) = [C(d_L, w; T; \lambda) - C(d_E, w; T; \lambda)]/L_L \quad (A6)$$

$$\Delta\mu_a^{\text{INTRA}}(T; \lambda) = \{ \ln[N(d_L, w_L; T; \lambda)/N_0(d_L, w_L; \lambda)] - \ln[N(d_E, w_E; T; \lambda)/N_0(d_E, w_E; \lambda)] + 1 \} / L_L \quad (A7)$$

1503 Finally, making the assumption that hemoglobin is the only chromo-
1505 phore contributing to absorption, $O_2\text{Hb}$ and HHb concentration changes
1506 are then derived by Lambert–Beer law, using the hemoglobin absorption
Q14507 spectra from Prahll (2013).

1508 Changes of moments of DTOFs are defined as in Liebert et al.
1509 (2004):

$$\Delta A(T; \lambda) = -\ln[N(T; \lambda)/N_0(\lambda)] \quad (A8)$$

$$\Delta \langle t(T; \lambda) \rangle = \langle t(T; \lambda) \rangle - \langle t_0(T; \lambda) \rangle \quad (A9)$$

$$\Delta V(T; \lambda) = V(T; \lambda) - V_0(T; \lambda) \quad (A10)$$

1513 where ΔA is the change in attenuation, N is the total number of pho-
1516 tons (0th order moment of DTOF, corresponding to the number of
1517 photons collected in a time window with delay 0 and width ∞), $\langle t \rangle$
1518 the mean photon time-of-flight (1st order moment) and V is the

variance (second centralized moment of the DTOF). The quantities
with index 0 refer to the signal recorded during a reference period
(e.g. the rest period before stimulation).

References

- Advanced Laser Diode Systems GmbH, 2013. PiLas. <http://www.alsgmbh.com/pilas.htm>. 1523
- Advanced Research Technologies (ART), 2013. Optix MX3 – pre-clinical optical molecular imager. <http://www.art.ca>. 1524
- Aguirre, A.D., Chen, Y., Fujimoto, J.G., Ruvinskaya, L., Devor, A., Boas, D.A., 2006. Depth-resolved imaging of functional activation in the rat cerebral cortex using optical coherence tomography. *Opt. Lett.* 31 (23), 3459–3461. 1526
- Alerstam, E., Andersson-Engels, S., Svensson, T., 2008a. Improved accuracy in time-resolved diffuse reflectance spectroscopy. *Opt. Express* 16 (14), 10440–10454. 1527
- Alerstam, E., Svensson, T., Andersson-Engels, S., 2008b. Parallel computing with graphics processing units for high-speed Monte Carlo simulation of photon migration. *J. Biomed. Opt.* 13 (6), 060504. 1528
- Aletti, F., Re, R., Pace, V., Contini, D., Molteni, E., Cerutti, S., Maria Bianchi, A., Torricelli, A., Spinelli, L., Cubeddu, R., Baselli, G., 2012. Deep and surface hemodynamic signal from functional time resolved transcranial near infrared spectroscopy compared to skin flowmotion. *Comput. Biol. Med.* 42 (3), 282–289. 1533
- Alphas GmbH, 2013. PICOPOWER™-LD Series. <http://www.alphas.com/products/lasers/picosecond-pulse-diode-lasers-with-driver-picopower-ld-series.html>. 1538
- Arridge, S.R., 1999. Optical tomography in medical imaging. *Inverse Prob.* 15, R41–R93. 1539
- Arridge, S.R., Schweiger, M., Hiraoka, M., Delpy, D.T., 1993. A finite element approach for modeling photon transport in tissue. *Med. Phys.* 20 (2), 299–309. 1540
- Arridge, S.R., Schweiger, M., Schotland, J.C., 2011. Inverse model in light transport. In: Boas, D.A., Pitrís, C., Ramanujam, N. (Eds.), *Handbook of Biomedical Optics, Part III, Chap. 17*. CRC Press, Boca Raton, Florida. 1541
- Aslin, R.N., 2013. Questioning the questions that have been asked about the infant brain using NIRS. *Cogn. Neuropsychol.* 29, 7–33. 1542
- Austin, T., Gibson, A.P., Branco, G., Yusuf, R.Md., Arridge, S.R., Meek, J.H., Wyatt, J.S., Delpy, D.T., Hebden, J.C., 2006. Three-dimensional optical imaging of blood volume and oxygenation in the preterm brain. *NeuroImage* 31 (4), 1426–1433. 1543
- Bari, V., Calcagnile, P., Molteni, E., Re, R., Contini, D., Spinelli, L., Caffini, M., Torricelli, A., Cubeddu, R., Cerutti, S., Bianchi, A.M., 2012. From neurovascular coupling to neurovascular cascade: a study on neural, autonomic and vascular transients in attention. *Physiol. Meas.* 33, 1379–1397. 1544
- Bassi, A., Brida, D., D'Andrea, C., Valentini, G., Cubeddu, R., De Silvestri, S., Cerullo, G., 2010. Time-gated optical projection tomography. *Opt. Lett.* 35, 2732–2734. 1545
- Becker, W., 2005. *Advanced Time-correlated Single-photon Counting*. Springer, Berlin, Heidelberg, New York. 1546
- Becker & Hickl GmbH, 2013a. BHL7-700. <http://www.becker-hickl.de/lasers.htm#BHL7-700>. 1547
- Becker & Hickl GmbH, 2013b. Detectors for photon counting. <http://www.becker-hickl.de/detectors.htm#HPM100-50>. 1548
- Becker & Hickl GmbH, 2013c. Simple-Tau 130 Table-Top TCSPC Systems. <http://www.becker-hickl.com/simpleTau.htm#st130>. 1549
- Becker & Hickl GmbH, 2013d. Time-correlated single photon counting devices. <http://www.becker-hickl.de/tcspc.htm>. 1550
- Benaron, D.A., Hintz, S.R., Villringer, A., Boas, D., Kleinschmidt, A., Frahm, J., Hirth, C., Obrig, H., van Houten, J.C., Kermit, E.L., 2000. Noninvasive functional imaging of human brain using light. *J. Cereb. Blood Flow Metab.* 20, 469–477. 1551
- Boas, D.A., Dale, A.M., 2005. Simulation study of magnetic resonance imaging-guided cortically constrained diffuse optical tomography of human brain function. *Appl. Opt.* 44 (10), 1957–1968. 1552
- Boas, D.A., O'Leary, M.A., Chance, B., Yodh, A.G., 1994. Scattering of diffuse photon density waves by spherical inhomogeneities within turbid media: analytic solution and applications. *Proc. Natl. Acad. Sci. U. S. A.* 91, 4887–4891. 1553
- Boas, D.A., Culver, J., Stott, J., Dunn, A., 2002. Three dimensional Monte Carlo code for photon migration through complex heterogeneous media including the adult human head. *Opt. Express* 10, 159–170. 1554
- Bodi, G., Bérubé-Lauzière, Y., 2009. A new deconvolution technique for time-domain signals in diffuse optical tomography without a priori information. *Proc. SPIE* 7369, 736914. 1555
- Brühl, R., Kummrow, A., Möller, M., Wabnitz, H., Liebert, A., Ittermann, B., Seifert, F., Rinneberg, H., 2005. Concurrent time-resolved near-infrared spectroscopy and fMRI measurements of visually stimulated humans. *Proceedings of the 13th Scientific Meeting and Exhibition of the International Society for Magnetic Resonance in Medicine (ISMRM)*, p. 499. 1556
- Busch, D.R., Choe, R., Durduran, T., Baker, W.B., Foster, E.K., Aversa, T.A., Friedman, D., Rosen, M.A., Schnall, M.D., Yodh, A.G., 2012. Microvascular blood flow changes in human breast during simulated mammography. *Biomedical Optics and 3D Imaging OSA 2012 (Paper JM3A.13)*. 1557
- Butti, M., Contini, D., Molteni, E., Caffini, M., Spinelli, L., Baselli, G., Bianchi, A.M., Cerutti, S., Cubeddu, R., Torricelli, A., 2009. Effect of prolonged stimulation on cerebral hemodynamic: a time-resolved fNIRS study. *Med. Phys.* 36, 4103–4114. 1558
- Canova, D., Roatta, S., Bosone, D., Micieli, G., 2011. Inconsistent detection of changes in cerebral blood volume by near infrared spectroscopy in standard clinical tests. *J. Appl. Physiol.* 110, 1646–1655. 1559
- Chance, B., Leigh, J.S., Miyake, H., Smith, D.S., Nioka, S., Greenfeld, R., Finander, M., Kaufmann, K., Levy, W., Young, M., Cohen, P., Yoshioka, H., Boretsky, R., 1988. Comparison of time-unresolved measurements of deoxyhemoglobin in brain. *Proc. Natl. Acad. Sci. U. S. A.* 85, 4971–4975. 1560

- 1601 Chen, G.N., Zhu, Q., 2002. Time-resolved optical measurements with spread spectrum
1602 excitation. *Opt. Lett.* 27 (20), 1806–1808.
- 1603 Chen, G.N., Zhu, Q., 2003. Time-resolved diffuse optical imaging using pseudo-
1604 random bit sequences. *Opt. Express* 11 (25), 3445–3454.
- 1605 Coherent Inc., 2013. Ultrafast Ti:sapphire oscillators. [http://www.coherent.com/
1606 Products/index.cfm?365/Ultrafast-Ti-Sapphire-Oscillators](http://www.coherent.com/Products/index.cfm?365/Ultrafast-Ti-Sapphire-Oscillators).
- 1607 Collins, D.L., Zijdenbos, A.P., Kollokian, V., Sled, J., Kabani, N., Holmes, C., Evans, A., 1998.
1608 Design and construction of a realistic digital brain phantom. *IEEE Trans. Med. Im-
1609 aging* 17 (3), 463–468.
- 1610 Contini, D., Torricelli, A., Pifferi, A., Spinelli, L., Paglia, F., Cubeddu, R., 2006.
1611 Multichannel time-resolved system for functional near infrared spectroscopy.
1612 *Opt. Express* 14, 5418–5432.
- 1613 Contini, D., Torricelli, A., Pifferi, A., Spinelli, L., Cubeddu, R., 2007. Novel method for depth-
1614 resolved brain functional imaging by time-domain NIRS. *Proc. SPIE* 6629, 662908.
- 1615 Contini, D., Spinelli, L., Caffini, M., Cubeddu, R., Torricelli, A., 2009. A multichannel time-
1616 domain brain oximeter for clinical studies. *Proc. SPIE* 7369, 73691D.
- 1617 Contini, D., Zucchelli, L., Spinelli, L., Caffini, M., Re, R., Pifferi, A., Cubeddu, R., Torricelli,
1618 A., 2012. Review: brain and muscle near infrared spectroscopy/imaging tech-
1619 niques. *J. Near Infrared Spectrosc.* 20 (1), 15–27.
- 1620 Contini, D., Dalla Mora, A., Di Sieno, L., Tosi, A., Boso, G., Torricelli, A., Spinelli, L.,
1621 Cubeddu, R., Pifferi, A., 2013a. Time resolved functional near infrared spectroscopy
1622 by means of time gated system at small interfiber distance. *Oral Communication at
1623 SPIE BIOS 2013 Conference 8578 Optical Tomography and Spectroscopy of Tissue
1624 X*, 3 February 2013, Paper 8578-82.
- 1625 Contini, D., Re, R., Turola, M., Spinelli, L., Romano, G., Cubeddu, R., Torricelli, A., 2013b.
1626 Multi-channel time-resolved functional near infrared spectroscopy system. *Oral
1627 Communication at SPIE BIOS 2013 Conference 8578 Optical Tomography and
1628 Spectroscopy of Tissue X*, 3 February 2013, Paper 8578-114.
- 1629 Cooper, R.J., Caffini, M., Dubb, J., Fang, Q., Custo, A., Tsuzuki, D., Fischl, B., Wells III, W.,
1630 Dan, I., Boas, D.A., 2012a. Validating atlas-guided DOT: a comparison of diffuse
1631 optical tomography informed by atlas and subject-specific anatomies. *NeuroImage*
1632 62 (3), 1999–2006.
- 1633 Cooper, R.J., Gagnon, L., Goldenholz, D., Boas, D.A., Greve, D.N., 2012b. The utility of
1634 near-infrared spectroscopy in the regression of low-frequency physiological
1635 noise from functional magnetic resonance imaging data. *NeuroImage* 59 (4),
1636 3128–3138.
- 1637 Cubeddu, R., Pifferi, A., Taroni, P., Torricelli, A., Valentini, G., 1996. Experimental test of
1638 theoretical models for time-resolved reflectance. *Med. Phys.* 23 (9), 1625–1633.
- 1639 Cubeddu, R., Pifferi, A., Taroni, P., Torricelli, A., Valentini, G., 1999. A compact tissue oximeter
1640 based on dual-wavelength multichannel time-resolved reflectance. *Appl. Opt.* 38,
1641 3670–3680.
- 1642 Custo, A., Boas, D.A., Tsuzuki, D., Dan, I., Mesquita, R., Fischl, B., Grimson, W.E.L., Wells III,
1643 W., 2010. Anatomical atlas-guided diffuse optical tomography of brain activation.
1644 *NeuroImage* 49, 561–567.
- 1645 D'Andrea, C., Comelli, D., Pifferi, A., Torricelli, A., Valentini, G., Cubeddu, R., 2003. Time-
1646 resolved optical imaging through turbid media using a fast data acquisition system
1647 based on a gated CCD camera. *J. Phys. D: Appl. Phys.* 36, 1675–1681.
- 1648 Dehaes, M., Gagnon, L., Lesage, F., Pelegrini-Issac, M., Vignaud, A., Valabregue, R., Grebe,
1649 R., Wallois, F., Benali, H., 2011a. Quantitative investigation of the effect of the extra-
1650 cerebral vasculature in diffuse optical imaging: a simulation study. *Biomed. Opt. Express* 2 (3),
1651 680–695.
- 1652 Dehaes, M., Grant, P.E., Sliva, D.D., Roche-Labarbe, N., Pienaar, R., Boas, D.A.,
1653 Franceschini, M.A., Selb, J., 2011b. Assessment of the frequency-domain multi-
1654 distance method to evaluate the brain optical properties: Monte Carlo simulations
1655 from neonate to adult. *Biomed. Opt. Express* 2 (3), 552–567.
- 1656 Del Bianco, S., Martelli, F., Zaccanti, G., 2002. Penetration depth of light re-emitted by a
1657 diffusive medium: theoretical and experimental investigation. *Phys. Med. Biol.* 47,
1658 4131–4144.
- 1659 Del Bianco, S., Martelli, F., Cignini, F., Zaccanti, G., Sansone, G., Pifferi, A., Torricelli, A.,
1660 Bassi, A., Taroni, P., Cubeddu, R., 2004. Liquid phantom for investigating light prop-
1661 agation through layered diffusive media. *Opt. Express* 12, 2102–2111.
- 1662 Delpy, D.T., Cope, M., van der Zee, P., Arridge, S., Wray, S., Wyatt, J., 1988. Estimation of
1663 optical pathlength through tissue from direct time of flight measurement. *Phys. Med. Biol.* 33,
1664 1433–1442.
- 1665 Diop, M., St Lawrence, K., 2012. Deconvolution method for recovering the photon
1666 time-of-flight distribution from time-resolved measurements. *Opt. Lett.* 37
1667 (12), 2358–2360.
- 1668 Diop, M., Tichauer, K.M., Elliott, J.T., Migues, M., Lee, T.Y., St Lawrence, K., 2010. Compar-
1669 ison of time-resolved and continuous-wave near-infrared techniques for measuring
1670 cerebral blood flow in piglets. *J. Biomed. Opt.* 15 (5), 057004.
- 1671 Diop, M., Verdecchia, K., Lee, T., St Lawrence, K., 2011. Calibration of diffuse correlation
1672 spectroscopy with a time-resolved near-infrared technique to yield absolute cerebral
1673 blood flow measurements. *Biomed. Opt. Express* 2 (7), 2068–2082.
- 1674 Dunn, A.K., Boas, D.A., 2000. Transport-based image reconstruction in turbid media
1675 with small source-detector separations. *Opt. Lett.* 25 (24), 1777–1779.
- 1676 Durduran, T., Choe, R., Baker, W.B., Yodh, A.G., 2010. Diffuse optics for tissue monitoring
1677 and tomography. *Rep. Prog. Phys.* 73 (076701) (43 pp).
- 1678 Eda, H., Oda, I., Ito, Y., Wada, Y., Oikawa, Y., Tsunazawa, Y., Takada, M., Tsuchiya, Y.,
1679 Yamashita, Y., Oda, M., Sassaroli, A., Yamada, Y., Tamura, M., 1999. Multichannel
1680 timeresolved optical tomographic imaging system. *Rev. Sci. Instrum.* 70, 3595–3602.
- 1681 Edinburgh Photonics, 2013. The EPL series, picosecond pulsed diode lasers. [http://
1682 www.edinburghphotonics.com/files/file/technical-specifications/EPL%20Series%20
1683 Flyer.pdf](http://www.edinburghphotonics.com/files/file/technical-specifications/EPL%20Series%20Flyer.pdf).
- 1684 Eggebrecht, A.T., White, B.R., Ferradal, S.L., Chen, C., Zhan, Y., Snyder, A.Z., Dehghani, H.,
1685 Culver, J.P., 2012. A quantitative spatial comparison of high-density diffuse optical
1686 tomography and fMRI cortical mapping. *NeuroImage* 61 (4), 1120–1128.
- Eggleton, B.J., Luther-Davies, B., Richardson, K., 2011. Chalcogenide photonics. *Nat. Photonics* 5,
1687 141–148.
- 1688 Enfield, L.C., Gibson, A.P., Everdell, N.L., Delpy, D.T., Schweiger, M., Arridge, S.R., Richardson,
1689 C., Keshtgar, M., Douek, M., Hebden, J.C., 2007. Three-dimensional time-resolved optical
1690 mammography of the uncompressed breast. *Appl. Opt.* 46, 3628–3638.
- 1691 Excelitas Technologies Corp., 2013. Single photon counting modules. [http://www.
1692 excelitas.com/Pages/Product/Single-Photon-Counting-Modules-SPCM.aspx](http://www.excelitas.com/Pages/Product/Single-Photon-Counting-Modules-SPCM.aspx).
- 1693 Fang, Q., 2010. Mesh-based Monte Carlo method using fast ray-tracing in Plücker coordi-
1694 nates. *Biomed. Opt. Express* 1 (1), 165–175.
- 1695 Fang, Q., Boas, D.A., 2009. Monte Carlo simulation of photon migration in 3D turbid media
1696 accelerated by graphics processing units. *Opt. Express* 17 (22), 20178–20190.
- 1697 Fang, Q., Kaeli, D.R., 2012. Accelerating mesh-based Monte Carlo method on modern
1698 CPU architectures. *Biomed. Opt. Express* 3 (12), 3223–3230.
- 1699 Fang, Z., Zhao, C.Z., 2012. Recent progress in silicon photonics: a review. *ISRN Optics* 2012 (2012),
1700 Article ID 428690.
- 1701 Farina, A., Bassi, A., Pifferi, A., Taroni, P., Comelli, D., Spinelli, L., Cubeddu, R., 2009. Bandpass
1702 effects in time-resolved diffuse spectroscopy. *Appl. Spectrosc.* 63 (1), 48–56.
- 1703 Feng, S., Zeng, F., Chance, B., 1995. Photon migration in the presence of a single defect:
1704 a perturbation analysis. *Appl. Opt.* 34 (19), 3826–3837.
- 1705 Ferrari, M., Quaresima, V., 2012. A brief review on the history of human functional
1706 near-infrared spectroscopy (fNIRS) development and fields of application. *NeuroImage* 63,
1707 921–935.
- 1708 Ferrari, M., De Blasi, R.A., Safoue, F., Wei, Q., Zaccanti, G., 1993. Towards human brain
1709 near infrared imaging: time resolved and unresolved spectroscopy during hypoxic
1710 hypoxia. *Adv. Exp. Med. Biol.* 333, 21–31.
- 1711 Ferrari, M., Norris, K.H., Sowa, M.G. (Eds.), 2012. *Medical Applications of NIR Spectroscopy: J. Near Infrared Spectrosc.*, vol. 20 (Issue 1).
1712 1713
- 1713 Fianium UK Ltd., 2013a. ALP (advanced laser platform). [http://www.fianium.com/alp.
1714 htm](http://www.fianium.com/alp.htm).
- 1715 Fianium UK Ltd., 2013b. WhiteLase SC sources and accessories. [http://www.fianium.
1716 com/supercontinuum.htm](http://www.fianium.com/supercontinuum.htm).
- 1717 Foschum, F., Fugger, O., Jäger, M., Simon, E., Kienle, A., Pifferi, A., Spinelli, L., Torricelli,
1718 A., Farina, A., Bargigia, I., Cubeddu, R., Jelzow, A., Wabnitz, H., Macdonald, R.,
1719 Martelli, F., Zaccanti, G., Heiskala, J., Arridge, S.R., Liebert, A., Sawosz, P., Milej, D.,
1720 2012. In vivo optical spectroscopy of the head. *Oral Communication to the
1721 nEUROpt Workshop, Non-invasive Imaging of Brain Function and Disease by
1722 Pulsed Near Infrared Light*, Milan, 12–13 March 2012.
- 1723 Frederick, B., Boas, D.A., 2013. <http://fnirs.org/software/>.
- 1724 Fujimoto, J.G., Brezinski, M.E., Tearney, G.J., Boppart, S.A., Bouma, B.E., Hee, M.R., Southern,
1725 J.F., Swanson, E.A., 1995. Optical biopsy and imaging using optical coherence tomog-
1726 raphy. *Nat. Methods* 1, 970–972.
- 1727 Fukui, Y., Ajichi, Y., Okada, E., 2003. Monte Carlo prediction of near-infrared light
1728 propagation in realistic adult and neonatal head models. *Appl. Opt.* 42, 2881–2887.
- 1729 Gagnon, L., Gauthier, C., Hoge, R.D., Lesage, F., 2008. Double-layer estimation of intra- and
1730 extracerebral hemoglobin concentration with a time-resolved system. *J. Biomed. Opt.* 13 (5),
1731 054019.
- 1732 Gagnon, L., Cooper, R.J., Yucel, M.A., Perdue, K.L., Greve, D.N., Boas, D.A., 2012a. Short
1733 separation channel location impacts the performance of short channel regression
1734 in NIRS. *NeuroImage* 59, 2518–2528.
- 1735 Gagnon, L., Yucel, M.A., Dehaes, M., Cooper, R.J., Perdue, K.L., Selb, J., Huppert, T.J., Hoge,
1736 R.D., Boas, D.A., 2012b. Quantification of the cortical contribution to the NIRS signal
1737 over the motor cortex using concurrent NIRS-fMRI measurements. *NeuroImage* 59,
1738 3933–3940.
- 1739 Gao, F., Zhao, H., Tanikawa, Y., Yamada, Y., 2004. Optical tomographic mapping of cerebral
1740 haemodynamics by means of time-domain detection: methodology and phantom
1741 validation. *Phys. Med. Biol.* 49 (2004), 1055–1078.
- 1742 Gerega, A., Milej, D., Weigl, W., Botwicz, M., Zolek, N., Kacprzak, M., Wierzejski, W.,
1743 Toczyłowska, B., Mayznar-Zawadzka, E., Maniewski, R., Liebert, A., 2012. Multiwavelength
1744 time-resolved detection of fluorescence during the inflow of indocyanine green into the
1745 adult's brain. *J. Biomed. Opt.* 17 (8), 87001.
- 1746 Gervain, J., Mehler, J., Werker, J.F., Nelson, C.A., Csibra, G., Lloyd-Fox, S., Shukla, M.,
1747 Aslin, R.A., 2011. Near-infrared spectroscopy: a report from the McDonnell infant
1748 methodology consortium. *Dev. Cogn. Neurosci.* 1, 22–46.
- 1749 Gibson, A.P., Austin, T., Everdell, N.L., Schweiger, M., Arridge, S.R., Meek, J.H., Wyatt, J.S.,
1750 Delpy, D.T., Hebden, J.C., 2006. Three-dimensional whole-head optical tomography
1751 of passive motor evoked responses. *NeuroImage* 30, 521–528.
- 1752 Golovko, D., Meier, R., Rummeny, E., Daldrup-Link, H., 2011. Optical imaging of rheuma-
1753 toid arthritis. *Int. J. Clin. Rheumatol.* 6 (1), 67–75.
- 1754 Gowar, J., 1993. *Optical Communication Systems*, 2nd edition. Prentice Hall, Hemel Hempstead.
1755 1756
- 1757 Hamamatsu Photonics, K.K., 2013a. Guide to streak camera. [http://sales.hamamatsu.
1758 com/assets/pdf/catsandguides/e_streakh.pdf](http://sales.hamamatsu.com/assets/pdf/catsandguides/e_streakh.pdf).
- 1759 Hamamatsu Photonics, K.K., 2013b. Microchannel plates. [http://sales.hamamatsu.
1760 com/en/products/electron-tube-division/detectors/microchannel-plates-mcps.
1761 php](http://sales.hamamatsu.com/en/products/electron-tube-division/detectors/microchannel-plates-mcps.php).
- 1762 Hamamatsu Photonics, K.K., 2013c. Photomultiplier modules. [http://sales.hamamatsu.
1763 com/en/products/electron-tube-division/detectors/photomultiplier-modules.php](http://sales.hamamatsu.com/en/products/electron-tube-division/detectors/photomultiplier-modules.php).
- 1764 Hamamatsu Photonics, K.K., 2013d. Picosecond light pulser. [http://sales.hamamatsu.
1765 com/assets/pdf/hpspdf/e_plp10.pdf](http://sales.hamamatsu.com/assets/pdf/hpspdf/e_plp10.pdf).
- 1766 Hamamatsu Photonics, K.K., 2013e. TRS-20. [http://jp.hamamatsu.com/products/life-
1767 science/1002/index_en.html](http://jp.hamamatsu.com/products/life-science/1002/index_en.html).
- 1768 Hebden, J.C., Gonzalez, F.M., Gibson, A., Hillman, E.M.C., Yusof, R.M., Everdell, N., Delpy,
1769 D.T., Zaccanti, G., Martelli, F., 2003. Assessment of an in situ temporal calibration
1770 method for time-resolved optical tomography. *J. Biomed. Opt.* 8 (1), 87–92.
- 1771 Hebden, J.C., Gibson, A.P., Austin, T., Yusof, R.M., Everdell, N., Delpy, D.T., Arridge, S.R.,
1772 Meek, J.H., Wyatt, J.S., 2004. Imaging changes in blood volume and oxygenation

- 1773 in the newborn infant brain using three-dimensional optical tomography. *Phys.*
1774 *Med. Biol.* 49 (7), 1117–1130.
- 1775 Hebden, J.C., Magazov, S., Everdell, N., Varela, M., 2012a. A time-domain system for optical
1776 tomography of the newborn infant brain. *Oral Communication to the nEUROpt Workshop, Non-invasive Imaging of Brain Function and Disease by*
1777 *Pulsed Near Infrared Light*, Milan, 12–13 March 2012.
- 1778 Hebden, J.C., Varela, M., Magazov, S., Everdell, N., Gibson, A., Meek, J., Austin, T.,
1779 2012b. Diffuse optical imaging of the newborn infant brain. *Proc. of 9th IEEE International Symposium, "Biomedical Imaging: from Nano to Macro"*, 2–5 May
1780 2012 (Barcelona).
- 1781 Hervé, L., Puszka, A., Planat-Chrétien, A., Dinten, J.M., 2012. Time-domain diffuse optical
1782 tomography processing by using the Mellin–Laplace transform. *Appl. Opt.* 51 (25),
1783 5978–5988.
- 1784 Hielscher, A.H., Klose, A.D., Beuthan, J., 2000. Evolution strategies for optical tomography
1785 characterization of homogeneous media. *Opt. Express* 7, 507–518.
- 1786 Hielscher, A.H., Kim, H.K., Klose, A.H., 2011. Forward models of light transport in biological
1787 tissue. In: Boas, D.A., Pitris, C., Ramanujam, N. (Eds.), *Handbook of Biomedical Optics, Part III*, Chap. 16. CRC Press, Boca Raton, Florida.
- 1788 Hillman, E.M.C., Boas, D.A., Dale, A.M., Dunn, A.K., 2004. Laminar optical tomography:
1789 demonstration of millimeter-scale depth-resolved imaging in turbid media. *Opt. Lett.* 29 (14), 1650–1652.
- 1790 Hillman, E.M.C., Amoozegar, C.B., Wang, T., McCaslin, A.F.H., Bouchard, M.B., Mansfield,
1791 J., Levenson, R.M., 2011. In vivo optical imaging and dynamic contrast methods for
1792 biomedical research. *Phil. Trans. R. Soc. A* 369, 4620–4643.
- 1793 Hintz, S.R., Benaron, D.A., van Houten, J.C., Duckworth, J.L., Liu, F.W.H., Spilman, S.D.,
1794 Stevenson, D.K., Cheong, W., 1998. Stationary headband for clinical time-of-flight
1795 optical imaging at the bedside. *Photochem. Photobiol.* 68 (3), 361–369.
- 1796 Ho, P.P., Baldeck, P., Wong, K.S., Yoo, K.M., Lee, D., Alfano, R.R., 1989. Time dynamics of
1797 photon migration in semiopaque random media. *Appl. Opt.* 28, 2304–2310.
- 1798 Hoshi, Y., Shinba, T., Sato, C., Doi, N., 2006. Resting hypofrontality in schizophrenia: a study
1799 using near-infrared time-resolved spectroscopy. *Schizophr. Res.* 84, 411–420.
- 1800 Hwang, J., Ramella-Roman, J., Nordstrom, R., 2012. Introduction: feature issue on phantoms
1801 for the performance evaluation and validation of optical medical imaging devices.
1802 *Biomed. Opt. Express* 3, 1399–1403.
- 1803 ID Quantique SA, 2013. id100 SERIES. [http://www.idquantique.com/instrumentation/
1804 product/id100-silicon-apd-single-photon-detector.html](http://www.idquantique.com/instrumentation/product/id100-silicon-apd-single-photon-detector.html).
- 1805 Ijichi, S., Kusaka, T., Isobe, K., Islam, F., Okubo, K., Okada, H., Namba, M., Kawada, K., Imai, T.,
1806 Itoh, S., 2005a. Quantification of cerebral hemoglobin as a function of oxygenation using
1807 near-infrared time-resolved spectroscopy in a piglet model of hypoxia. *J. Biomed. Opt.* 10 (2), 024026.
- 1808 Ijichi, S., Kusaka, T., Isobe, K., Okubo, K., Kawada, K., Namba, M., Okada, H., Nishida, T.,
1809 Imai, T., Itoh, S., 2005b. Developmental changes of optical properties in neonates
1810 determined by near-infrared time-resolved spectroscopy. *Pediatr. Res.* 58 (3),
1811 568–573.
- 1812 Ijichi, S., Kusaka, T., Isobe, K., Okubo, K., Yasuda, S., Kawada, K., Itoh, S., 2005c. Developmental
1813 changes of optical properties in infants determined by near-infrared time-resolved
1814 spectroscopy. *J. Cereb. Blood Flow Metab.* 25, S228.
- 1815 International Electrotechnical Commission, 2001. IEC 60825-1, Edition 1.2. Safety of
1816 Laser Products – Part 1: Equipment Classification, Requirements and User's Guide.
- 1817 International Electrotechnical Commission, 2013. IEC 80601-2-71 Ed. 1.0. Medical electrical
1818 equipment – Part 2-71: particular requirements for the basic safety and essential
1819 performance of functional oximeter equipment. [http://www.iec.ch/dyn/
1820 www/?p=103:38:0:::FSP_ORG_ID,FSP_APEX_PAGE,FSP_LANG_ID,FSP_PROJECT:
1821 1365,23,25,IEC%2080601-2-71%20Ed.%201.0](http://www.iec.ch/dyn/www/?p=103:38:0:::FSP_ORG_ID,FSP_APEX_PAGE,FSP_LANG_ID,FSP_PROJECT:1365,23,25,IEC%2080601-2-71%20Ed.%201.0).
- 1822 Intes, X., 2005. Time-domain optical mammography SoftScan; initial results. *Acad. Radiol.* 12, 934–947.
- 1823 Jacques, S.L., 1989a. Time resolved propagation of ultrashort laser pulses within turbid
1824 tissues. *Appl. Opt.* 28, 2223–2239.
- 1825 Jacques, S.L., 1989b. Time-resolved reflectance spectroscopy in turbid tissues. *IEEE
1826 Trans. Biomed. Eng.* 36, 1155–1161.
- 1827 Jelzow, A., Kirilina, E., Wabnitz, H., Kummrow, A., Bruehl, R., Ittermann, B.,
1828 Macdonald, R., 2009. Towards improved quantification of functional activation
1829 in human brain by concurrent fMRI and time-resolved NIRS. 446. WE-Heraeus-
1830 Seminar "Optical Imaging of Brain Function" December 7th–10th, 2009, Bad
1831 Honnef, Germany.
- 1832 Jelzow, A., Koch, S., Wabnitz, H., Steinbrink, J., Obrig, H., Macdonald, R., 2010. Combined
1833 EEG and time-resolved NIRS to study neurovascular coupling in the adult brain. *International Summer School on Multimodal Approaches in Neuroscience July 19th–21st,
1834 2010 (Leipzig, Germany)*.
- 1835 Jelzow, A., Wabnitz, H., Obrig, H., Macdonald, R., Steinbrink, J., 2012. Separation of
1836 indocyanine green boluses in the human brain and scalp based on time-resolved
1837 in-vivo fluorescence measurements. *J. Biomed. Opt.* 17 (5), 057003.
- 1838 Kacprzak, M., Liebert, A., Sawosz, P., Zolek, N., Maniewski, R., 2007. Time-resolved optical
1839 imager for assessment of cerebral oxygenation. *J. Biomed. Opt.* 12, 034019.
- 1840 Kacprzak, M., Liebert, A., Staszkievicz, W., Gabrusiewicz, A., Sawosz, P., Madycki, G.,
1841 Maniewski, R., 2012. Application of a time-resolved optical brain imager for monitoring
1842 cerebral oxygenation during carotid surgery. *J. Biomed. Opt.* 17 (1), 016002.
- 1843 Kakahana, Y., Kiyonaga, N., Yasuda, T., Imabayashi, T., Ohryoji, T., Nakahara, M., Okayama,
1844 N., Kanmura, Y., Kikuchi, T., Yonemitsu, T., 2010. Dynamic changes in cerebral oxygenation
1845 by two methods during cardiac surgery and postoperative cognitive decline. *Crit. Care* 14 (Suppl. 1), P334.
- 1846 Kakahana, Y., Okayama, N., Matsunaga, A., Yasuda, T., Imabayashi, T., Nakahara, M.,
1847 Kiyonaga, N., Ikoma, K., Kikuchi, T., Kanmura, Y., Oda, M., Ohmae, E., Suzuki, T.,
1848 Yamashita, Y., Tamura, M., 2012. Cerebral monitoring using near-infrared time-resolved
1849 spectroscopy and postoperative cognitive dysfunction. *Adv. Exp. Med. Biol.* 737, 19–24.
- 1850 Kiguchi, M., Ichikawa, N., Atsumori, H., Kawaguchi, F., Sato, H., Maki, A., Koizumi, H., 2007. 1850
1851 Comparison of light intensity on the brain surface due to laser exposure during optical
1852 tomography and solar irradiation. *J. Biomed. Opt.* 12 (6), 062108.
- 1853 Kirilina, E., Jelzow, A., Heine, A., Niessing, M., Wabnitz, H., Brühl, R., Ittermann, B.,
1854 Jacobs, A.M., Tachtsidis, I., 2012. The physiological origin of task-evoked systemic
1855 artefacts in functional near infrared spectroscopy. *NeuroImage* 61 (1), 70–81.
- 1856 Kuga, Y., Ishimaru, A., Bruckner, A.P., 1983. Experiments on picosecond pulse propagation
1857 in a diffuse medium. *J. Opt. Soc. Am. A* 73, 1812–1815.
- 1858 Lapointe, E., Pichette, J., Bérubé-Lauzière, Y., 2012. A multi-view time-domain non-
1859 contact diffuse optical tomography scanner with dual wavelength detection for intrinsic
1860 and fluorescence small animal imaging. *Rev. Sci. Instrum.* 83, 063703.
- 1861 LaVision BioTec GmbH, 2013. Ultra-fast gated cameras. [http://www.lavision.de/
1862 products/cameras/ultrafast_gated_cameras.php](http://www.lavision.de/products/cameras/ultrafast_gated_cameras.php).
- 1863 Liebert, A., Wabnitz, H., Grosenick, D., Macdonald, R., 2003. Fiber dispersion in time domain
1864 measurements compromising the accuracy of determination of optical properties
1865 of strongly scattering media. *J. Biomed. Opt.* 8 (3), 512–516.
- 1866 Liebert, A., Wabnitz, H., Steinbrink, J., Obrig, H., Möller, M., Macdonald, R., Villringer, A.,
1867 Rinneberg, H., 2004. Time-resolved multidistance near-infrared spectroscopy of the
1868 adult head: intracerebral and extracerebral absorption changes from moments
1869 of distribution of times of flight of photons. *Appl. Opt.* 43 (15), 3037–3047.
- 1870 Liebert, A., Wabnitz, H., Steinbrink, J., Möller, M., Macdonald, R., Rinneberg, H.,
1871 Villringer, A., Obrig, H., 2005. Bed-side assessment of cerebral perfusion in stroke
1872 patients based on optical monitoring of a dye bolus by time-resolved diffuse reflectance.
1873 *NeuroImage* 24 (2), 426–435.
- 1874 Liebert, A., Wabnitz, H., Obrig, H., Erdmann, R., Möller, M., Macdonald, R., Rinneberg,
1875 H., Villringer, A., Steinbrink, J., 2006. Non-invasive detection of fluorescence from
1876 exogenous chromophores in the adult human brain. *NeuroImage* 31 (2),
1877 600–608.
- 1878 Liebert, A., Sawosz, P., Milej, D., Kacprzak, M., Weigl, W., Botwicz, M., Mączewska, J.,
1879 Fronczewska, K., Mayzner-Zawadzka, E., Królicki, L., Maniewski, R., 2011. Assessment
1880 of inflow and washout of indocyanine green in the adult human brain by
1881 monitoring of diffuse reflectance at large source–detector separation. *J. Biomed. Opt.* 16 (4), 046011.
- 1882 Liebert, A., Wabnitz, H., Elster, C., 2012. Determination of absorption changes from moments
1883 of distributions of times of flight of photons: optimization of measurement
1884 conditions for a two-layered tissue model. *J. Biomed. Opt.* 17 (5), 057005.
- 1885 Liemert, A., Kienle, A., 2012. Green's function of the time-dependent radiative transport
1886 equation in terms of rotated spherical harmonics. *Phys. Rev. E* 86, 036603.
- 1887 Liu, Y., Zhang, X., 2011. Metamaterials: a new frontier of science and technology. *Chem. Soc. Rev.* 40, 2494–2507.
- 1888 Maas, A.I.R., Citerio, G., 2010. Noninvasive monitoring of cerebral oxygenation in traumatic
1889 brain injury: a mix of doubts and hope. *Intensive Care Med.* 36, 1283–1285.
- 1890 Mackert, B., Leistner, S., Sander, Tilmann, Liebert, A., Wabnitz, H., Burghoff, M., Trahms,
1891 L., Macdonald, R., Curio, G., 2008. Dynamics of cortical neurovascular coupling analyzed
1892 by simultaneous DC-magnetoencephalography and time-resolved near-infrared
1893 spectroscopy. *NeuroImage* 39 (3), 979–986.
- 1894 Martelli, F., Del Bianco, S., Zaccanti, G., 2003. Procedure for retrieving the optical properties
1895 of a two-layered medium from time-resolved reflectance measurements. *Opt. Lett.* 28 (14), 1236–1238.
- 1896 Martelli, F., Del Bianco, S., Zaccanti, G., Pifferi, A., Torricelli, A., Bassi, A., Taroni, P.,
1897 Cubeddu, R., 2004. Phantom validation and in vivo application of an inversion procedure
1898 for retrieving the optical properties of diffusive layered media from time-resolved
1899 reflectance measurements. *Opt. Lett.* 29 (17), 2037–2039.
- 1900 Martelli, F., Del Bianco, S., Ismaelli, A., Zaccanti, G., 2009. Light Propagation through Biological
1901 Tissue and Other Diffusive Media: Theory, Solutions, and Software. SPIE Press, Washington, USA.
- 1902 Martelli, F., Del Bianco, S., Zaccanti, G., 2012. Retrieval procedure for time-resolved
1903 near-infrared tissue spectroscopy based on the optimal estimation method. *Phys. Med. Biol.* 57 (10), 2915–2929 (May 21).
- 1904 Mata Pavia, J., Charbon, E., Wolf, M., 2011a. 3D near-infrared imaging based on a single-photon
1905 avalanche diode array sensor. *Proc. SPIE* 8088, 808811.
- 1906 Mata Pavia, J., Niclass, C., Favi, C., Wolf, M., Charbon, E., 2011b. 3D near-infrared imaging
1907 based on a SPAD image sensor. *International Image Sensor Workshop (IISW), Hokkaido, Japan, 08 June 2011–11 June 2011*, p. R42.
- 1908 Mata Pavia, J., Charbon, E., Wolf, M., 2012. 3D near-infrared imaging based on a single-photon
1909 avalanche diode array sensor: a new perspective on reconstruction algorithms. *Conference Paper, Biomedical Optics, Miami, Florida, April 28, 2012*,
1910 Nevel Techniques and Models (BW1A), BW1A.5.
- 1911 Mazurenka, M., Jelzow, A., Wabnitz, H., Contini, D., Spinelli, L., Pifferi, A., Cubeddu, R.,
1912 Dalla Mora, A., Tosi, A., Zappa, F., Macdonald, R., 2012. Non-contact time-resolved
1913 diffuse reflectance imaging at null source–detector separation. *Opt. Express* 20 (1), 283–290.
- 1914 Mazurenka, M., Di Sieno, L., Boso, G., Contini, D., Pifferi, A., Dalla Mora, A., Tosi, A.,
1915 Wabnitz, H., Macdonald, R., 2013. Development of an optical non-contact time-resolved
1916 diffuse reflectance scanning imaging system: first in vivo tests. *Oral Communication at SPIE BioS 2013 Conference 8578 Optical Tomography and Spectroscopy of Tissue X, 6 February 2013, Paper 8578-88*.
- 1917 MCML, 2013. <http://omlc.ogi.edu/software/mc/>.
- 1918 Micro Photon Devices, 2013a. PDM series. [http://www.micro-photon-devices.com/
1919 products_pdm.asp](http://www.micro-photon-devices.com/products_pdm.asp).
- 1920 Micro Photon Devices, 2013b. PDM-R series. [http://www.micro-photon-devices.com/
1921 products_pdm-r.asp](http://www.micro-photon-devices.com/products_pdm-r.asp).
- 1922 Micro Photon Devices, 2013c. SPC2 series. [http://www.micro-photon-devices.com/
1923 products_spc2.asp](http://www.micro-photon-devices.com/products_spc2.asp).
- 1924 Milej, D., Gerega, A., Zolek, N., Weigl, W., Kacprzak, M., Sawosz, P., Mączewska, J.,
1925 Fronczewska, K., Mayzner-Zawadzka, E., Królicki, L., Maniewski, R., Liebert, A., 1944

- 1945 2012. Time-resolved detection of fluorescent light during inflow of ICG to the brain
1946 –a methodological study. *Phys. Med. Biol.* 57 (20), 6725–6742.
- 1947 Molteni, E., Contini, D., Caffini, M., Baselli, G., Spinelli, L., Cubeddu, R., Cerutti, S.,
1948 Bianchi, A.M., Torricelli, A., 2012. Load-dependent brain activation assessed by
1949 time-domain functional near-infrared spectroscopy during a working memory
1950 task with graded levels of difficulty. *J. Biomed. Opt.* 17 (5), 056005.
- 1951 Montcel, B., Poulet, P., 2006. An instrument for small-animal imaging using time-
1952 resolved diffuse and fluorescence optical methods. *Nucl. Instrum. Methods Phys.*
1953 *Res., Sect. A* 569 (2), 551–556.
- 1954 Montcel, B., Chabrier, R., Poulet, P., 2005. Detection of cortical activation with time-
1955 resolved diffuse optical methods. *Appl. Opt.* 44 (10), 1942–1947.
- 1956 Montcel, B., Chabrier, R., Poulet, P., 2006. Time-resolved absorption and hemoglobin
1957 concentration difference maps: a method to retrieve depth-related information
1958 on cerebral hemodynamics. *Opt. Express* 14 (25), 12271–12287.
- 1959 Moreira-Gonzalez, A., Papay, F.E., Zins, J.E., 2006. Calvarial thickness and its relation to
1960 cranial bone harvest. *Plast. Reconstr. Surg.* 117 (6), 1964–1971.
- 1961 Mottin, S., Montcel, B., de Chatellus, H.G., Ramstein, S., 2011. Functional white-laser im-
1962 aging to study brain oxygen uncoupling/recoupling in songbirds. *J. Cereb. Blood*
1963 *Flow Metab.* 31 (2), 393–400.
- 1964 Newport Corporation, 2013. Ultrafast lasers. [http://www.newport.com/Ultrafast-](http://www.newport.com/Ultrafast-Lasers/989320/1033/content.aspx)
1965 [Lasers/989320/1033/content.aspx](http://www.newport.com/Ultrafast-Lasers/989320/1033/content.aspx).
- 1966 Niedre, M.J., Turner, G.M., Ntziachristos, V., 2006. Time-resolved imaging of optical co-
1967 efficients through murine chest cavities. *J. Biomed. Opt.* 11 (1), 064017.
- 1968 NIRFAST, 2013. <http://www.dartmouth.edu/~nir/nirfast/>.
- 1969 NKT Photonics, 2013a. Large Mode Area (LMA) fibers. [http://www.nktpotonics.com/](http://www.nktpotonics.com/lmafibers-specifications)
1970 [lmafibers-specifications](http://www.nktpotonics.com/lmafibers-specifications).
- 1971 NKT Photonics, 2013b. SuperK supercontinuum sources. [http://www.nktpotonics.com/](http://www.nktpotonics.com/supercontinuum_sources)
1972 [supercontinuum_sources](http://www.nktpotonics.com/supercontinuum_sources).
- 1973 Nomura, Y., Hazekiy, O., Tamura, M., 1997. Relationship between time-resolved and
1974 non-time-resolved Beer–Lambert law in turbid media. *Phys. Med. Biol.* 42,
1975 1009–1022.
- 1976 Ntziachristos, V., Ma, X., Yodh, A.G., Chance, B., 1999. Multichannel photon counting
1977 instrument for spatially resolved near infrared spectroscopy. *Rev. Sci. Instrum.* 70
1978 (1), 193–201.
- 1979 O'Connor, D.V., Phillips, D., 1984. *Time Correlated Single Photon Counting*. Academic
1980 Press, London.
- 1981 Obrig, H., Hirth, C., Ruben, J., Dirnagl, U., Villringer, A., Wabnitz, H., Grossebeck, D.,
1982 Rinneberg, H., 1996. Near-infrared spectroscopy in functional activation studies:
1983 new approaches. *NeuroImage* 3 (Suppl. 1), S 403.
- 1984 Oda, M., Yamashita, Y., Nakano, T., Suzuki, A., Shimizu, K., Hirano, I., Shimomura, F.,
1985 Ohmae, E., Suzuki, T., Tsuchiya, Y., 1999. Near infrared time-resolved spectroscopy
1986 system for tissue oxygenation monitor. *Proc. SPIE* 3597, 611–617.
- 1987 Oda, M., Ohmae, E., Suzuki, H., Suzuki, T., Yamashita, Y., 2009. Tissue oxygenation mea-
1988 surements using near-infrared time-resolved spectroscopy. *J. Jpn. Coll. Angiol.* 49,
1989 131–137.
- 1990 Ohmae, E., Ouchi, Y., Oda, M., Suzuki, T., Nobesawa, S., Kanno, T., Yoshikawa, E.,
1991 Futatsubashi, M., Ueda, Y., Okada, H., Yamashita, Y., 2006. Cerebral hemodynamics
1992 evaluation by near-infrared time-resolved spectroscopy: correlation with simulta-
1993 neous positron emission tomography measurements. *NeuroImage* 29, 697–705.
- 1994 Ohmae, E., Oda, M., Suzuki, T., Yamashita, Y., Kakihana, Y., Matsunaga, A., Kanmura, Y.,
1995 Tamura, M., 2007. Clinical evaluation of time-resolved spectroscopy by measuring
1996 cerebral hemodynamics during cardiopulmonary bypass surgery. *J. Biomed. Opt.*
1997 12 (6), 062112.
- 1998 Okamoto, M., Dan, H., Sakamoto, K., Takeo, K., Shimizu, K., Kohno, S., Oda, I., Isobe, S.,
1999 Suzuki, T., Kohyama, K., Dan, I., 2004. Three-dimensional probabilistic anatomical
2000 cranio-cerebral correlation via the international 10–20 system oriented for trans-
2001 cranial functional brain mapping. *NeuroImage* 21, 99–111.
- 2002 Patterson, M.S., Chance, B., Wilson, B.C., 1989. Time resolved reflectance and transmit-
2003 tance for the non-invasive measurement of tissue optical properties. *Appl. Opt.* 28,
2004 2331–2336.
- 2005 PicoQuant GmbH, 2013a. Hybrid photomultiplier detector assembly. <http://www.picoquant.com/products/hpd/hpd.htm>.
- 2006 PicoQuant GmbH, 2013b. LDH series. [http://www.picoquant.com/products/ldh/ldhseries.](http://www.picoquant.com/products/ldh/ldhseries.htm)
2007 [htm](http://www.picoquant.com/products/ldh/ldhseries.htm).
- 2008 PicoQuant GmbH, 2013c. LDH-FA series. [http://www.picoquant.de/products/ldh_fa/](http://www.picoquant.de/products/ldh_fa/ldh_fa.htm)
2009 [ldh_fa.htm](http://www.picoquant.de/products/ldh_fa/ldh_fa.htm).
- 2010 PicoQuant GmbH, 2013d. Multichannel picosecond event timer & TCSPC module.
2011 <http://www.picoquant.com/products/hydrarharp400/hydrarharp400.htm>.
- 2012 PicoQuant GmbH, 2013e. Single photon counting module. [http://www.picoquant.com/](http://www.picoquant.com/products/tau_spad/tau_spad.htm)
2013 [products/tau_spad/tau_spad.htm](http://www.picoquant.com/products/tau_spad/tau_spad.htm).
- 2014 Pifferi, A., Torricelli, A., Taroni, P., Cubeddu, R., 2001. Reconstruction of absorber con-
2015 centrations in a two-layer structure by use of multidistance time-resolved reflectance
2016 spectroscopy. *Opt. Lett.* 26 (24), 1963–1965.
- 2017 Pifferi, A., Torricelli, A., Bassi, A., Taroni, P., Cubeddu, R., Wabnitz, H., Grossebeck, D.,
2018 Möller, M., MacDonald, R., Swartling, J., Svendsen, T., Andersson-Engels, S., van
2019 Veen, R.L.P., Sterenborg, H.J.C.M., Tualle, J., Nghiem, H.L., Avriplier, S., Whelan, M.,
2020 Stamm, H., 2005. Performance assessment of photon migration instruments: the
2021 MEDPHOT protocol. *Appl. Opt.* 44, 2104–2114.
- 2022 Pifferi, A., Torricelli, A., Spinelli, L., Contini, D., Cubeddu, R., Martelli, F., Zaccanti, G., Tosi,
2023 A., Dalla Mora, A., Zappa, F., Cova, S., 2008. Time-resolved diffuse reflectance at null
2024 source–detector separation using a fast gated single-photon avalanche diode. *Phys.*
2025 *Rev. Lett.* 100, 138101.
- 2026 Pifferi, A., Contini, D., Spinelli, L., Torricelli, A., Cubeddu, R., Martelli, F., Zaccanti, G.,
2027 Dalla Mora, A., Tosi, A., Zappa, F., 2010. The spread matrix: a method to predict
2028 the effect of a non time-invariant measurement system. *Biomedical Optics, OSA*
2029 *Technical Digest (CD)*. Optical Society of America, pp. 1–3 (paper BSu222).
- Prahl, S., 2013. Optical absorption of hemoglobin. [http://omlc.ogi.edu/spectra/](http://omlc.ogi.edu/spectra/hemoglobin/index.html) 2031
[hemoglobin/index.html](http://omlc.ogi.edu/spectra/hemoglobin/index.html). 2032
- Quaresima, V., Ferrari, M., Torricelli, A., Spinelli, L., Pifferi, A., Cubeddu, R., 2005. Bilateral
2033 prefrontal cortex oxygenation responses to a verbal fluency task: a multichannel
2034 time-resolved near-infrared topography study. *J. Biomed. Opt.* 10, 11012. 2035
- Re, R., Contini, D., Caffini, M., Cubeddu, R., Spinelli, L., Torricelli, A., 2010. A compact
2036 time-resolved system for near infrared spectroscopy based on wavelength space
2037 multiplexing. *Rev. Sci. Instrum.* 81 (11), 113101. 2038
- Ren, N., Liang, J., Qu, X., Li, J., Lu, B., Tian, J., 2010. GPU-based Monte Carlo simulation for
2039 light propagation in complex heterogeneous tissues. *Opt. Express* 18 (7), 6811–6823. 2040
- Saager, R.B., Telleri, N.L., Berger, A.J., 2011. Two-detector Corrected Near Infrared Spectro-
2041 scopy (C-NIRS) detects hemodynamic activation responses more robustly than
2042 single-detector NIRS. *NeuroImage* 55 (4), 1679–1685. 2043
- Sander, T.H., Liebert, A., Mackert, B.M., Wabnitz, H., Leistner, S., Curio, G., Burghoff, M.,
2044 Macdonald, R., Trahms, L., 2007. DC-magnetoencephalography and time-resolved
2045 near-infrared spectroscopy combined to study neuronal and vascular brain re-
2046 sponses. *Physiol. Meas.* 28 (6), 651–664. 2047
- Sassaroli, A., Martelli, F., 2012. Equivalence of four Monte Carlo methods for photon mi-
2048 gration in turbid media. *JOSA A* 29 (10), 2110–2117. 2049
- Sassaroli, A., Martelli, F., Fantini, S., 2010. Perturbation theory for the diffusion equation
2050 by use of the moments of the generalized temporal point-spread function. III.
2051 Frequency-domain and time-domain results. *JOSA A* 27 (7), 1723–1742. 2052
- Sato, C., Yamaguchi, T., Seida, M., Ota, Y., Yu, I., Iguchi, Y., Nemoto, M., Hoshi, Y., 2007.
2053 Intraoperative monitoring of depth dependent hemoglobin concentration changes dur-
2054 ing carotid endarterectomy by time-resolved spectroscopy. *Appl. Opt.* 46 (14), 2785–2792. 2055
- Sawosz, P., Kacprzak, M., Zolek, N., Weigl, W., Wojtkiewicz, S., Maniewski, R., Liebert, A.,
2056 2010. Optical system based on time-gated, intensified charge-coupled device camera
2057 for brain imaging studies. *J. Biomed. Opt.* 15 (6), 066025. 2058
- Sawosz, P., Zolek, N., Kacprzak, M., Maniewski, R., Liebert, A., 2012. Application of time-
2059 gated CCD camera with image intensifier in contactless detection of absorbing in-
2060 clusions buried in optically turbid medium which mimics local changes in oxygena-
2061 tion of the brain tissue. *Opto-Electron. Rev.* 20 (4), 309–314. 2062
- Scarpa, F., Brigadói, S., Cutini, S., Scatturin, P., Zorzi, M., Dell'Acqua, R., Sparacino, G.,
2063 2013. A reference-channel based methodology to improve estimation of event re-
2064 lated hemodynamic response from fNIRS measurements. *NeuroImage*. [http://](http://dx.doi.org/10.1016/j.neuroimage.2013.01.021)
2065 dx.doi.org/10.1016/j.neuroimage.2013.01.021 (in press). 2066
- Schmidt, F.E.W., Fry, M.E., Hillman, E.M.C., Hebdén, J.C., Delpy, D.T., 2000. A32-channel
2067 time resolved instrument for medical optical tomography. *Rev. Sci. Instrum.*
2068 71, 256–265. 2069
- Selb, J., Boas, D.A., 2012. A second generation time-domain imaging system from MGH.
2070 Oral Communication to the nEUROPT Workshop, Non-invasive Imaging of Brain
2071 Function and Disease by Pulsed Near Infrared Light, Milan, 12–13 March 2012. 2072
- Selb, J., Gibson, A., 2011. Diffuse optical tomography: time domain. In: Boas, D.A., Pitris,
2073 C., Ramanujan, N. (Eds.), *Handbook of Biomedical Optics, Part III*, Chap. 20. CRC
2074 Press, Boca Raton, Florida. 2075
- Selb, J., Stott, J.J., Franceschini, M.A., Sorensen, A.G., Boas, D.A., 2005. Improved sensitivity
2076 to cerebral hemodynamics during brain activation with a time-gated optical system:
2077 analytical model and experimental validation. *J. Biomed. Opt.* 10 (1), 11013. 2078
- Selb, J., Joseph, D.K., Boas, D.A., 2006. Time-gated optical system for depth-resolved
2079 functional brain imaging. *J. Biomed. Opt.* 11, 044008. 2080
- Selb, J., Dale, A., Boas, D.A., 2007. Linear 3D reconstruction of time-domain diffuse opti-
2081 cal imaging differential data: improved depth localization and lateral resolution.
2082 *Opt. Express* 15, 16400–16412. 2083
- Selb, J., Zimmermann, B.B., Martino, M., Ogden, T.M., Boas, D.A., 2013. Functional brain
2084 imaging with a supercontinuum time-domain NIRS system. Oral Communication
2085 at SPIE BIOS 2013 Conference 8578 Optical Tomography and Spectroscopy of Tis-
2086 sue X, 3 February 2013, Paper 8578-7. 2087
- SensL, 2013a. Measurement instruments. [http://sensl.com/products/measurement-](http://sensl.com/products/measurement-instruments/)
2088 [instruments/](http://sensl.com/products/measurement-instruments/). 2089
- SensL, 2013b. Photon counting systems. [http://sensl.com/products/photon-counting-](http://sensl.com/products/photon-counting-systems/)
2090 [systems/](http://sensl.com/products/photon-counting-systems/). 2091
- Siesler, H.W., Ozaki, Y., Kawata, S., Heise, H.M. (Eds.), 2002. *Near-infrared Spectroscopy: Principles, Instruments, Apps*. Wiley-VCH Verlag GmbH, Weinheim
2092 (Germany). 2093
- Simon, E., Foschum, F., Kienle, A., 2013. Hybrid Green's function of the time-dependent
2094 radiative transfer equation for anisotropically scattering semi-infinite media.
2095 *J. Biomed. Opt.* 18 (1), 015001. 2096
- Spinelli, L., Martelli, F., Del Bianco, S., Pifferi, A., Torricelli, A., Cubeddu, R., Zaccanti, G.,
2097 2006. Absorption and scattering perturbations in homogeneous and layered diffu-
2098 sive media probed by time-resolved reflectance at null source–detector separation.
2099 *Phys. Rev. E* 74, 021919. 2100
- Spinelli, L., Martelli, F., Torricelli, A., Pifferi, A., Zaccanti, G., 2009a. Nonlinear fitting procedure
2101 for accurate time-resolved measurements in diffusive media. *Proc. SPIE* 7369, 73691C. 2102
- Spinelli, L., Pifferi, A., Contini, D., Cubeddu, R., Torricelli, A., 2009b. Time-resolved opti-
2103 cal stratigraphy in turbid media. *Proc. SPIE* 7371, 73710A. 2104
- Steinbrink, J., Wabnitz, H., Obrig, H., Villringer, A., Rinneberg, H., 2001. Determining
2105 changes in NIR absorption using a layered model of the human head. *Phys. Med.*
2106 *Biol.* 46, 879–896. 2107
- Steinkellner, O., Gruber, C., Wabnitz, H., Jelzow, A., Steinbrink, J., Fiebach, J.B.,
2108 Macdonald, R., Obrig, H., 2010. Optical bedside monitoring of cerebral perfusion:
2109 technological and methodological advances applied in a study on acute ischemic
2110 stroke. *J. Biomed. Opt.* 15 (6), 061708. 2111
- Steinkellner, O., Jelzow, A., Wabnitz, H., Macdonald, R., 2012. A time-domain brain im-
2112 ager for various clinical applications. Oral Communication to the nEUROPT Work-
2113 shop, Non-invasive Imaging of Brain Function and Disease by Pulsed Near
2114 Infrared Light, Milan, 12–13 March 2012. 2115
- 2116

- 2117 Takahashi, T., Takikawa, Y., Kawagoe, R., Shibuya, S., Iwano, T., Kitazawa, S., 2011. Influence of skin blood flow on near-infrared spectroscopy signals measured on the forehead during a verbal fluency task. *NeuroImage* 57, 991–1002.
- 2118
- 2119
- 2120 Taroni, P., Pifferi, A., Quarto, G., Spinelli, L., Torricelli, A., Cubeddu, R., 2012. Chapter 9, diffuse optical imaging: application to breast imaging. In: Anastasio, A., La Riviere, P. (Eds.), *Emerging Imaging Technologies in Medicine*. CRC Press, Boca Raton, Florida.
- 2121
- 2122 TOAST, 2013. <http://web4.cs.ucl.ac.uk/research/vis/toast/index.html>.
- 2123
- 2124 Tolguenec, G.L., Lantz, E., Devaux, F., 1997. Imaging through scattering media by parametric amplification of images: study of the resolution and the signal-to-noise ratio. *Appl. Opt.* 36, 8292–8297.
- 2125
- 2126
- 2127 Toninelli, C., Vekris, E., Ozin, G.A., John, S., Wiersma, D.S., 2008. Exceptional reduction of the diffusion constant in partially disordered photonic crystals. *Phys. Rev. Lett.* 101, 123901.
- 2128
- 2129 Torricelli, A., Pifferi, A., Taroni, P., Giambattistelli, E., Cubeddu, R., 2001. In vivo optical characterization of human tissues from 610 to 1010 nm by time-resolved reflectance spectroscopy. *Phys. Med. Biol.* 46, 2227–2237.
- 2130
- 2131 Torricelli, A., Quaresima, V., Pifferi, A., Biscotti, G., Spinelli, L., Taroni, P., Ferrari, M., Cubeddu, R., 2004. Mapping of calf muscle oxygenation and haemoglobin content during dynamic plantar flexion exercise by multi-channel time-resolved near infrared spectroscopy. *Phys. Med. Biol.* 49, 685–699.
- 2132
- 2133 Torricelli, A., Pifferi, A., Spinelli, L., Cubeddu, R., Martelli, F., Del Bianco, S., Zaccanti, G., 2005. Time-resolved reflectance at null source-detector separation: improving contrast and resolution in diffuse optical imaging. *Phys. Rev. Lett.* 95, 078101.
- 2134
- 2135 Torricelli, A., Contini, D., Pifferi, A., Spinelli, L., Cubeddu, R., Nocetti, L., Manginelli, A.A., Baraldi, P., 2007. Simultaneous acquisition of time-domain fNIRS and fMRI during motor activity. *Proc. SPIE* 6631, 66310A.
- 2136
- 2137 Torricelli, A., Contini, D., Caffini, M., Zucchelli, L., Cubeddu, R., Spinelli, L., Molteni, E., Bianchi, A.M., Baselli, G., Cerutti, S., Visani, E., Gilioli, I., Rossi Sebastiano, D., Schiaffi, E., Panzica, F., Franceschetti, S., 2011. Assessment of cortical response during motor task in adults by a multimodality approach based on fNIRS–EEG, fMRI–EEG, and TMS. *Proc. SPIE* 8088, 808802.
- 2138
- 2139 Tosi, A., Dalla Mora, A., Zappa, F., Gulinatti, A., Contini, D., Pifferi, A., Spinelli, L., Torricelli, A., Cubeddu, R., 2011. Fast-gated single-photon counting technique widens dynamic range and speeds up acquisition time in time-resolved measurements. *Opt. Express* 19 (11), 10735–10746.
- 2140
- 2141 Tsuzuki, D., Jurcak, V., Singh, A.K., Okamoto, M., Watanabe, E., Dan, I., 2007. Virtual spatial registration of stand-alone fNIRS data to MNI space. *NeuroImage* 34 (4), 1506–1518.
- 2142
- 2143 Tsuzuki, D., Cai, D.S., Dan, H., Kyutoku, Y., Fujita, A., Watanabe, E., Dan, I., 2012. Stable and convenient spatial registration of stand-alone NIRS data through anchor-based probabilistic registration. *Neurosci. Res.* 72 (2), 163–171.
- 2144
- 2145 Tuchin, V., 2010. *Handbook of Photonics for Biomedical Science*. CRC Press, Taylor & Francis Group, London.
- 2146
- 2147 Ueda, Y., Yamanaka, T., Yamashita, D., Suzuki, T., Ohmae, E., Oda, M., Yamashita, Y., 2005. Reflectance diffuse optical tomography: its application to human brain mapping. *Jpn. J. Appl. Phys.* 44, 1203–1206.
- 2148
- 2149 van der Zee, P., Cope, M., Arridge, S.R., Essenpreis, M., Potter, L.A., Edwards, A.D., Wyatt, J.S., McCormick, D.C., Roth, S.C., Reynolds, E.O., 1992. Experimentally measured optical pathlengths for the adult head, calf and forearm and the head of the newborn infant as a function of inter optode spacing. *Adv. Exp. Med. Biol.* 316, 143–153.
- 2150
- 2151 Vignal, C., Boumans, T., Montcel, B., Ramstein, S., Verhoye, M., Van Audekerke, J., Mathevon, N., Van der Linden, A., Mottin, S., 2008. Measuring brain hemodynamic changes in a songbird: responses to hypercapnia measured with functional MRI and near-infrared spectroscopy. *Phys. Med. Biol.* 53 (10), 2457–2470.
- 2152
- 2153 Wabnitz, H., Möller, M., Liebert, A., Walter, A., Erdmann, R., Raitza, O., Drenckhahn, C., Dreier, J., Obrig, H., Steinbrink, J., Macdonald, R., 2005. A time-domain NIR brain imager applied in functional stimulation experiments. *Proc. OSA-SPIE Biomed. Opt. Presented at the Photon Migration and Diffuse-Light Imaging II*, pp. 70–78.
- 2154
- 2155 Wabnitz, H., Möller, M., Liebert, A., Obrig, H., Steinbrink, J., Macdonald, R., 2010. Time-resolved near-infrared spectroscopy and imaging of the adult human brain. *Adv. Exp. Med. Biol.* 662, 143–148.
- 2156
- 2157 Wabnitz, H., Pifferi, A., Torricelli, A., Taubert, D.R., Mazurenka, M., Steinkellner, O., Jelzow, A., Farina, A., Bargigia, I., Contini, D., Caffini, M., Zucchelli, L., Spinelli, L., Sawosz, P., Liebert, A., Macdonald, R., Cubeddu, R., 2011. Assessment of basic instrumental performance of time-domain optical brain imagers. *Proc. SPIE* 7896, 789602.
- 2158
- 2159 Wabnitz, H., Jelzow, A., Mazurenka, M., Steinkellner, O., Taubert, D.R., Macdonald, R., Pifferi, A., Torricelli, A., Contini, D., Zucchelli, L., Spinelli, L., Cubeddu, R., Milej, D., Zolek, N., Kacprzak, M., Sawosz, P., Liebert, A., Magazov, A., Hebden, J.C., Martelli, F., Di Ninni, P., Zaccanti, G., 2013. Performance assessment of time-domain optical brain imagers: a multi-laboratory study. Invited Paper at SPIE BIOS 2013 Conference 8578 Optical Tomography and Spectroscopy of Tissue X, 3 February 2013, Paper 8583–21.
- 2160
- 2161 Wang, L., Ho, P.P., Liu, C., Zhang, G., Alfano, R.R., 1991. Ballistic 2-d imaging through scattering walls using an ultrafast optical Kerr gate. *Science* 253, 769–771.
- 2162
- 2163 Wang, L., Jacques, S.L., Zheng, L.-Q., 1995. MCML – Monte Carlo modeling of photon transport in multi-layered tissues. *Comput. Methods Programs Biomed.* 47, 131–146.
- 2164
- 2165 Wolf, M., Ferrari, M., Quaresima, V., 2007. Progress of near-infrared spectroscopy and topography for brain and muscle clinical applications. *J. Biomed. Opt.* 12, 062104.
- 2166
- 2167 Wyatt, J.S., Cope, M., Delpy, D.T., van der Zee, P., Arridge, S., Edwards, A.D., Reynolds, E.O., 1990. Measurement of optical path length for cerebral near-infrared spectroscopy in newborn infants. *Dev. Neurosci.* 12, 140–144.
- 2168
- 2169 Yamashita, D., Yamanaka, T., Suzuki, T., Ohmae, E., Ueda, Y., Oda, M., Yamashita, Y., 2003. Development of multi-channel time resolved spectroscopy system and application of this system to measurement of brain function. *Proc. Opt. Jpn. Symp. Biomed. Opt.* 3, 72–73.
- 2170
- 2171 Yokose, N., Sakatani, K., Murata, Y., Awano, T., Igarashi, T., Nakamura, S., Hoshino, T., Katayama, Y., 2010. Bed-side monitoring of cerebral blood oxygenation and hemodynamics after aneurysmal subarachnoid hemorrhage by quantitative time-resolved near infrared spectroscopy. *World Neurosurg.* 73, 508–513.
- 2172
- 2173 Yucel, M.A., Huppert, T.J., Boas, D.A., Gagnon, L., 2012. Calibrating the BOLD signal during a motor task using an extended fusion model incorporating DOT, BOLD and ASL data. *NeuroImage* 61 (4), 1268–1276.
- 2174
- 2175 Zhao, Q., Spinelli, L., Torricelli, A., Cubeddu, R., Pifferi, A., 2010. Reconstruction in diffuse optical tomography using genetic algorithm. Conference Paper Biomedical Optics, Sunday Poster Session (BSuD), Miami, Florida, April 11, 2010.
- 2176
- 2177 Zhao, Q., Spinelli, L., Bassi, A., Valentini, G., Contini, D., Torricelli, A., Cubeddu, R., Zaccanti, G., Martelli, F., Pifferi, A., 2011. Functional tomography using a time-gated ICCD camera. *Biomed. Opt. Express* 2 (3), 705–716.
- 2178
- 2179
- 2180
- 2181
- 2182
- 2183
- 2184
- 2185
- 2186
- 2187
- 2188
- 2189
- 2190
- 2191
- 2192
- 2193
- 2194
- 2195
- 2196
- 2197
- 2198
- 2199
- 2200
- 2201
- 2202
- 2203
- 2204
- 2205
- 2206
- 2207
- 2208
- 2209
- 2210
- 2211
- 2212
- 2213

2214